https://doi.org/10.5194/hess-2020-243
Preprint. Discussion started: 30 July 2020


Hydrology and Earth System Sciences
Discussions
Open Access
EGU

# Targets-specified grids-tailored sub-model approach for fast large-scale high-resolution 2D urban flood modelling

Guohan Zhao [a,*], Thomas Balstrøm [a], Ole Mark [b], Marina B. Jensen [a]

[a] Department of Geoscience and Natural Resource Management, University of Copenhagen, Rolighedsvej 23, 1958 Frederiksberg C, Denmark

[b] DHI, Agern Allé 5, DK-2970 Hørsholm, Denmark

*Corresponding author. E-mail address: gz@ign.ku.dk.

## Graphic abstract

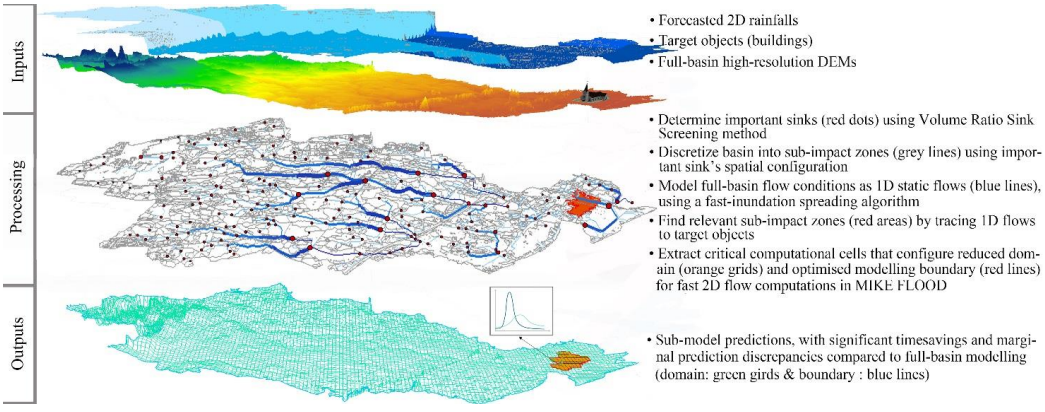


## Abstract

The accuracy of two-dimensional urban flood models (2D models) is improved when high-resolution Digital Elevation Models (DEMs) is used, but the entailed high spatial discretisation results in excessive computational expenses, thus prohibiting the use of 2D models in real-time forecasting at a large scale. This paper presents a sub-model approach to tailoring high-resolution 2D model grids according to specified targets, and thus such tailor-made sub-model yields fast processing without significant loss of accuracy. Among the numerous sinks detected from full-basin high-resolution DEMs, the computationally important ones are determined using a proposed Volume Ratio Sink Screening method. Also, the drainage basin is discretised into a collection of sub-impact zones according to those sinks' spatial configuration. When adding full-basin distributed static rainfall, the drainage basin's flow conditions are modelled as a "1D static flow" by using a fast-inundation spreading algorithm. Next, sub-impact zones relevant to the targets' local inundation process

https://doi.org/10.5194/hess-2020-243
Preprint. Discussion started: 30 July 2020


Hydrology and Earth System Sciences
Discussions

can be identified by tracing the 1D flow continuity, and thus suggest the critical computational cells from the high-resolution model grids on the basis of the spatial intersection. In MIKE FLOOD's 2D simulations, those screened cells configure the reduced computational domains as well as the optimised boundary conditions, which ultimately enables the fast 2D prediction in the tailor-made sub-model. To validate the method, model experiments were designed to test the impact of the reduced computational domains and the optimised boundary conditions separately. Further, the general applicability and the robustness of the sub-model approach were evaluated by targeting at four focus areas representing different catchment terrain morphologies as well as different rainfall return periods of 1-100 years. The sub-model approach resulted in a 45-553 times faster processing with a 99% reduction in the number of computational cells for all four cases; the predicted flood extents, depths and flow velocities showed only marginal discrepancies with Root Mean Square Errors (RMSE) below 1.5 cm. As such, this approach reduces the 2D models' computing expenses significantly, thus paving the way for large-scale high-resolution 2D real-time forecasting.

**Keywords**: Targets-specified modelling, tailored grids, sub-model generation, large-scale high-resolution flood modelling, real-time forecasting.

https://doi.org/10.5194/hess-2020-243
Preprint. Discussion started: 30 July 2020


Hydrology and Earth System Sciences
Discussions

## 1. Introduction

Urban floods pose escalating threats to human settlements in times of continued urbanisation and climate change (Bernstein et al., 2008). In order to mitigate the flood risks and the related consequences, a flood forecasting system that complies with two criteria: i) accurate spatial and temporal flood predictions and ii) sufficient lead time between rainfall predictions and flood predictions, is considered as a prerequisite to provide precise early warnings for decision makers. Therefore, with the purpose of identifying an accurate and timely urban flood model to configure such a system, we review two types of models: i) 2D hydrodynamic models (Section 1.1) and ii) 1D static models (Section 1.2). After summarising the strengths and potentials for the two models, the scientific innovation of the proposed approach is outlined by identifying a 1D/2D complementary solution that adapts a 1D static model to tailor a 2D model grids based on specified targets, thus achieving fast and accurate predictions in large-scale high-resolution 2D urban flood modelling (Section 1.3).

### 1.1 2D hydrodynamic models (2D models)

By enabling more realistic 2D dynamic flows across regular grids, 2D models are advocated as a preferential approach to other alternatives for urban flood simulations (Maksimović et al., 2009; Mark et al., 2004; Mark and Parkinson, 2005; Schmitt et al., 2004; Leandro et al., 2009). However, 2D models tend to be computationally expensive. When numerical solvers (implicit/explicit solvers) are executed in a high spatial discretisation based on a fine grid, to stabilise the models, the optimum time steps must be decreased accordingly, which boost processing time considerably. Although applying a coarse grid is considered a straightforward way to reduce computing time, it turns out that the extra details inherent in high-resolution DEMs can benefit simulation accuracy substantially (Fewtrell et al., 2008; Yu and Lane, 2006a). Particularly when micro-topography dominates the direction of flood propagation, grid coarsening may smear critical elevation information resulting in imprecise inundation distributions (Fewtrell et al., 2011; Jensen et al., 2010). Recently, the occurrence of decimetric DEMs allows for the inclusion of more detailed micro-topographies in urban flood models, which initiates a new high-resolution simulation era. However, due to the prohibitive processing time, high-resolution applications have been limited to small scale modelling only (Fewtrell et al., 2011; Sampson et al., 2012). For the same reason, the use of high-resolution grids in real-time forecasts

https://doi.org/10.5194/hess-2020-243
Preprint. Discussion started: 30 July 2020


Hydrology and Earth System Sciences
Discussions

(nowcasting) is impractical. Consequently, applying high-resolution DEMs to large-scale modelling and real-time forecasts remains a challenge.

To improve the 2D models' computational efficiency, four speed-up approaches may be employed: i) parallelization technology taking advantage of Graphics Processing Units (GPUs), multi-core Central Processing Units (MCs), remotely distributed computers and cloud computing such as JFLOW-GPU (Lamb et al., 2009), OpenMP (Neal et al., 2009), MPI libraries (Neal et al., 2010), FloodMap-Paraller model (Yu, 2010) and CityCAT (Glenis et al., 2013); ii) a simplified hydrodynamic model approach that solves simplified governing equations, whereby reasonable flood extents and depths can be yielded quickly although the momentum conservation is less emphasized, e.g. inertial LISFLOOD-FP (Bates et al., 2010) and Quasi 2D (Kuiry et al., 2010); iii) a coarse-grid approach, where computational time is reduced by increasing the grid size (Yu and Lane, 2006a); to compensate for loss of accuracy due to smearing of details, especially around buildings, various improvements have been introduced, including sub-grid treatment (Chen et al., 2012a; Yu and Lane, 2006b; Yu and Lane, 2011), the multi-cell approach (Hénonin et al., 2015), the multi-layered approach (Chen et al., 2012b) and the porosity parameter (Bruwier et al., 2017; Guinot and Soares-Frazão, 2006; McMillan and Brasington, 2007; Sanders et al., 2008); and iv) the Cellular Automata (CA) approach, where a universal transition rule is coded for spatial discretization in the simulation, thus achieving a reduced-complexity procedure in 2D models (Dottori and Todini, 2010; Dottori and Todini, 2011; Ghimire et al., 2013; Guidolin et al., 2016). Whereas these technologies may reduce computational costs to some extent, new fast-approaching remote sensing technologies delivering enhanced data accuracy in tremendous volumes are even more difficult for them to handle (Bates et al., 1997; Barnea and Filin, 2008; Cobby et al., 2003; Fewtrell et al., 2011; Leitão, 2016; Lichti et al., 2008; Marks and Bates, 2000; Mason et al., 2003; Mason et al., 2007; Meesuk et al., 2015; Sampson et al., 2012; Schubert et al., 2008; Tokarczyk et al., 2015). Especially, the use of a high-resolution modelling grid is the precondition to explicitly include all detailed spatial representations of datasets into 2D simulations. Thus, the computational efficiency of 2D models remains a challenge in the high-resolution data context.

https://doi.org/10.5194/hess-2020-243
Preprint. Discussion started: 30 July 2020


Hydrology and Earth System Sciences
Discussions

### 1.2 1D static models (fast-inundation spreading models)

Although 2D hydrodynamic models still dominate, increasing attention is paid towards fast-inundation spreading models due to their fast computing speed. Noteworthy examples include RFIM (Krupka et al., 2007; Liu and Pender, 2010, Jamali et al., 2018), RFSM (Bernini and Franchini, 2013; Gouldby et al., 2008; Lhomme et al., 2008), ISIS-FAST (Shaad, 2009), FCDC (Zhang et al., 2014), GUFIM (Chen et al., 2009), SCALGO (Arge et al., 2010), USISM (Zhang and Pan, 2014) and Arc-Malstrøm (Balstrøm and Crawford, 2018). A conception of "hydrostatic condition" (Bernini and Franchini, 2013), also known as the "flat water assumption" (Zerger et al., 2002) is commonly embedded as the underlying algorithm in these models. With mass conservation as the only governing law and disregarding temporal evolution, the fast-inundation spreading models present a filling/spilling process within the predefined flow patterns thus resulting in predictions rapidly. Here, we name the process "1D static flow" in this research. These models are divided into two types (Zhang and Pan, 2014): one is used for point-source triggered floodings like dam breaching and riverbank overflow (RFIM, RFSM, ISIS-FAST, FCDC); the other (non-point source models) is more directly relevant to stormwater-inundations in urban areas (GUFIM, USISM, Arc-Malstrøm). By using 1D static flows instead of 2D dynamic flows the fast inundation spreading models gain computational efficiency substantially, and thus a fast-processing speed is obtained particularly when dealing with large-scale high-resolution DEMs. However, there are two notable drawbacks: first of all, due to their intrinsic neglect of time evolution, they cannot reproduce flow dynamics (i.e. hydrographs), and peaks may be miss-captured in such static simulations. Secondly, they do not account for the conservation of momentum and, therefore, cannot provide flow velocities, which is essential to flood risk assessments.

### 1.3 Hypothesis and research objectives

The simplified urban flood models can be designed to perform specific modelling tasks by deliberately ignoring the representation processes deemed incidental to the defined modelling purpose (Hunter et al., 2007). If we adapt a 1D static model to exclude 2D model grids that are irrelevant to specified targets (i.e. specified buildings and specified precipitations), then 2D dynamic flows would avoid the prohibitive processing time

https://doi.org/10.5194/hess-2020-243
Preprint. Discussion started: 30 July 2020


Hydrology and Earth System Sciences
Discussions

when dealing with large-scale high-resolution DEMs, while compensating for the drawbacks of 1D static flows used, which results in cost-efficient tailor-made sub-models.

This paper presents a sub-model approach to reducing 2D models' computing time in case of large-scale high-resolution urban flood modelling. The reduction is done by two phases (I/II) distinguished by multiple scales (i.e. basin/local catchment), see Fig. 1: i) aiming at identifying reduced domains, the 1D static model (Arc-Malstrøm) is adapted to trace the relevant sub-impact zones based on specified target objects and specified precipitations; ii) aiming at the highest precise flow predictions, the full 2D dynamic model (MIKE FLOOD) is used based on the reduced domain intersected with sub-impact zones. To investigate the influence of the domain reductions, the MIKE FLOOD predictions based on the sub-model domain is benchmarked against the one of the full domain, and further compared to the one defined from municipality borders. Meanwhile, to investigate the validity of the suggested boundary conditions, the discrepancies of optimal boundary condition is compared to the ones of uniform closed-/open-boundary conditions. Finally, to prove general applicability and robustness, performances of four sub-models are benchmarked and compared using different terrain morphologies as well as different rainfall return periods.

## 2. Methodology

The program of the sub-model approach is adapted from the prototype of Arc-Malstrøm and consists of five modules (Modules I-V, as illustrated in Fig. 1), where Module II is essentially following the Arc-Malstrøm and Modules I, III-V is added for the sub-model tailoring purpose. The general procedure is programmed and wrapped up with ArcGIS' Python interface (ArcPy). To address the distinctions between Arc-Malstrøm and the sub-model approach, further comparisons and associated tests are inclosed as Supplementary Document S1, S2 and S3.

https://doi.org/10.5194/hess-2020-243
Preprint. Discussion started: 30 July 2020


Hydrology and Earth System Sciences
Discussions

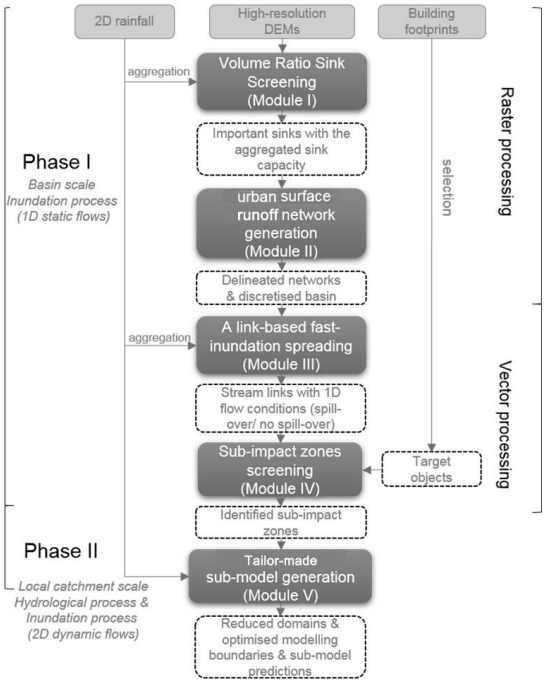


Fig. 1. Illustration of the suggested method. In the central column, shaded boxes represent major modules; light grey boxes are required input data; dashed-line boxes are intermediate data between different modules and the final outputs. Phase I and Phase II (left side) represent the two major phases, where an appropriate level of modelling complexities (hydrological/inundation process) is addressed at each modelling scale (basin/local catchment scale) to achieve a holistic computational efficiency in multiple-scale simulations. The right side represents the GIS processing environment that shifts from raster (computationally expensive) to vector processing (computationally cheap) for the sake of the general computational expense reduction.

### 2.1 Volume ratio sink screening (Module I)

When creating an urban surface runoff network, the numbers and spatial configuration of sinks are critical factors concerning network delineations (stream links) and discretisation of the drainage basin. To avoid spurious network components due to an increasing number of sinks detected from high-resolution DEMs (i.e. 0.4 m/1.6 m), a Volume Ratio Sink Screening method (VRSS) is proposed as presented in Fig. 2a. This module screens for computationally important sinks to generate relevant networks (Section 2.2) and adequate volumes involved in subsequent computations (Section 2.3).

https://doi.org/10.5194/hess-2020-243
Preprint. Discussion started: 30 July 2020


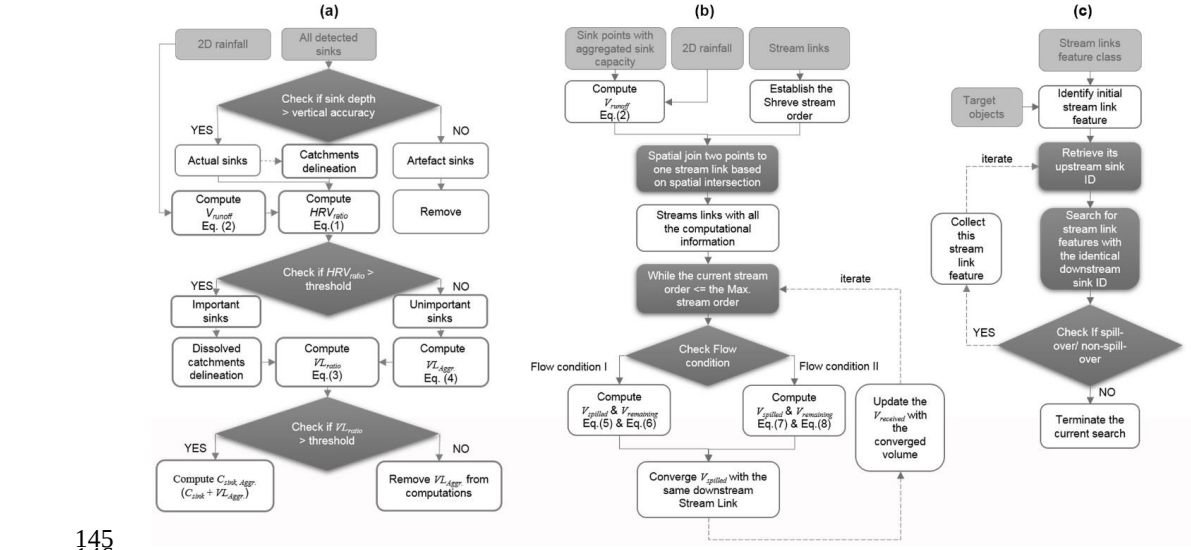


Fig. 2. (a) The Volume Ratio Sink Screening method; (b) The link-based fast-inundation spreading algorithm; (c) The sub-impact zones screening method, where the dark grey shaded boxes represent major steps and light grey boxes are input data. Note: $V_{runoff}$ – Runoff Volume, $HRV_{ratio}$ – Hydrological Retention Volume ratio, $VL_{Aggr.}$ – Aggregated Volume Loss, $VL_{ratio}$ – Volume Loss ratio, $C_{sink, Aggr.}$ – Aggregated Sink Capacity, $V_{spilled}$ – Spilled Volume, $V_{remaining}$ – Remaining Volume, $V_{received}$ – Received Volume.

In general, sinks are classified into two categories: actual sinks and artefacts (Lindsay and Creed, 2006). To preserve the actual sinks only, the DEM's vertical accuracy is used, whereby artefact sinks shallower than or equal to this threshold value are removed. Other sink artefacts, such as detected inside enclosed building blocks or on rooftops, are deleted (see Fig. 3a). Nevertheless, the inclusion of all actual sinks as computational nodes may lead to massive computational costs while improving minor modelling accuracy for network-based computations (i.e. 1D static/dynamic modelling). To further differentiate "important" from "unimportant" sinks in light of the computational efficiency, the Hydrological Retention Volume Ratio ( $HRV_{ratio}$ ) is defined as the ratio between a sink's capacity (volume) and the runoff volume generated from its associated contributing catchment, which reflects the sink's runoff retention performance (strong/poor) relative to rainfall amounts, see Eq. (1) and (2). So, if we consider the spill-over as a transition moment when a sink uses up all retention capacities and generates runoff only, then "unimportant" sinks that make quicker spill-over during a rain event should be modelled as part of catchments rather than having retention capacities. To substitute those catchments from screened "unimportant" sinks, "important" sinks should initiate another round of catchment delineation (drainage basin discretisation) resulting in "dissolved catchments", see Fig. 3b.

https://doi.org/10.5194/hess-2020-243
Preprint. Discussion started: 30 July 2020


Hydrology and Earth System Sciences
Discussions
Open Access
EGU

$$HRV_{ratio} = \frac{C_{sink}}{V_{runoff}} = \frac{S_1}{S_1 + S_2} \quad (1)$$

$$V_{runoff} = R_{cellsize}{}^2 \times \sum_{i=1}^{n} A_i \quad (2)$$

where $C_{sink}$ is the sink's capacity; $R_{cellsize}$ is the cell size of the 2D rainfall (distributed dynamic rainfall) that has the commensurate cell size of DEMs; $A_i$ is the total rainfall contained by cell $i$ in the total rainfall raster (distributed static rainfall) that is aggregated from the 2D rainfall, and $n$ is the total number of rainfall cells within each sink's catchment. $S_1$ and $S_2$ are the accumulated rainfall from the hyetograph before and after the unimportant sinks start spilling over. This means that an equivalent proportion is shared between this volume ratio and the percentile of the rainfall hyetograph. Therefore, to determine such a parameter, the accumulated rainfall amount that indicates a spilling moment for the unimportant sinks can act as a reference.

Since volume losses associated with removed "unimportant" sinks may accumulate to significant volume due to stream branch convergences, the Volume Loss Ratio ($VL_{ratio}$), see Eq. (3), is introduced. This ratio is defined as the aggregated volume loss in removed sinks vs. the downstream "important" sinks' retention capacities. The aggregated volume loss is calculated as shown in Eq. (4) and depends on the volume and number of "unimportant" sinks. If the aggregated volume loss is relatively high compared to the important sinks included, it cannot be ignored but is added to the downstream important sinks' capacities. Otherwise, insignificant volumes are removed. In this way, the computationally important number of sinks and their aggregated sink capacities ($C_{sink,\ Aggr.}$) are determined with VRSS.

$$VL_{ratio} = \frac{VL_{Aggr.}}{C_{sink}} \quad (3)$$

$$VL_{Aggr.} = \sum_{i=1}^{n} V_i \quad (4)$$

https://doi.org/10.5194/hess-2020-243
Preprint. Discussion started: 30 July 2020


Hydrology and Earth System Sciences
Discussions
Open Access
EGU

where $VL_{Aggr.}$ is the aggregated volume losses; $V_i$ is the volume loss from the identified "unimportant" sink *i*, and *n* is the number of sinks located within the dissolved catchment (see Fig. 3b).

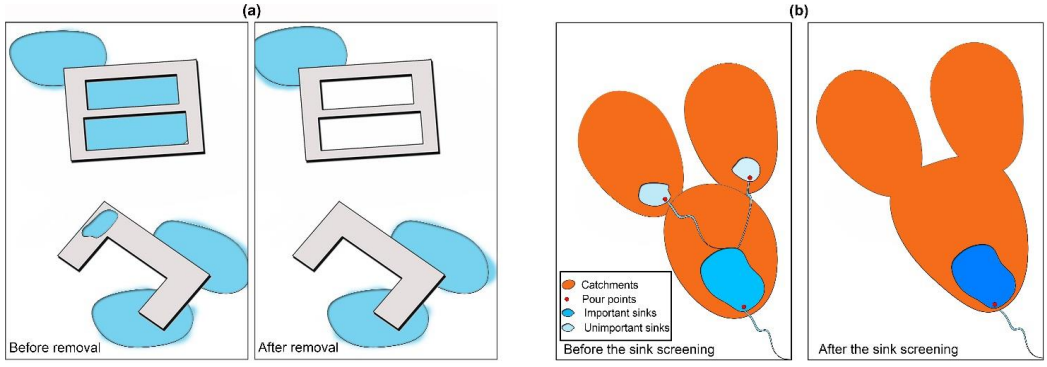


Fig. 3. (a) Artefact sinks on roofs and within enclosed buildings (left), and after removal (right); (b) Sink screening process where unimportant sinks (light blue, left) are removed and important sinks (dark blue, left) are selected to delineate one dissolved catchment (right). Besides, volumes from unimportant sinks (removed, right) are summarized as the $VL_{Aggr.}$ to be added to the capacity of the important sink (dark blue, right) downstream. Finally, the important sink with $C_{sink,\ Aggr.}$ (dark blue, right) is generated. Note: pour points (red) denote the starting points of concentrated flow from sheet-flow (orange area) to channel-flow (blue line); the gradually darker blue colour (right) represents the enlarged capacity due to the volume aggregation.

The suggested VRSS method offers several advantages over other alternatives (Maksimović et al. 2009, Balstrøm and Crawford, 2018). First, instead of conventional screening criteria (i.e. depth and volume) which reflects a geometric distinction between "small" and "big", sinks' runoff retention performance (poor/strong) is assessed to determine sinks' computational importance in network-based computations. Second, unlike absolute screening criteria, introducing the relative variable $V_{runoff}$ computed from the distributed total rainfall raster allows an adaptive sink screening criterion to be scaled with the spatially varying magnitude of precipitation, thus adding an effect of rainfall heterogeneity to the sink screening process. Third, sinks' pour points can denote a starting point of concentrated runoff, thus distinguishing runoff transition processes from sheet-flow to channel-flow, see Fig. 3(b). With an adaptive threshold value to differentiate these two flow conditions, a more precise hydraulic representation of catchment processes in 1D hydrodynamic models can be obtained. Fourth and finally, the volumes from screened sinks are not neglected. Instead, a criterion is applied to control the volume loss independent from the screening process of sink numbers. This can minimize the accumulated effect of volume losses throughout a basin-wise hierarchical network.

https://doi.org/10.5194/hess-2020-243
Preprint. Discussion started: 30 July 2020




206 **2.2 Urban surface runoff network generation (Module II)**

207 To assemble the urban surface runoff network (Fig. 4), we used the GIS-based method developed by Balstrøm
208 and Crawford (2018), including four hydro-objects: blue spots (sinks), their sub-impact zones (catchments),
209 their pour points, and stream links. "Blue spots" referring to all surface depressions (Hansson, 2010) are
210 generated by subtracting the original DEM from the filled DEM. "Sub-impact zones" describes the blue spots'
211 catchments identified by the ArcGIS' Watershed tool, where the discretization of the drainage basin is obtained
212 by the flow direction raster derived from the "8N approach" (Baker and Cai, 1992; Greenlee, 1987; Jenson
213 and Domingue, 1988). Pour points denote the overflow positions along the blue spots' rims, and their locations
214 are determined by searching for the highest flow accumulation cell value within each blue spot region as well
215 as the lowest elevation cell value along the rim. "Stream links" describes the topological connectivity between
216 blue spots, i.e. flow paths, and are delineated based on ArcGIS' Cost Path tool. Notably, the flow direction and
217 flow accumulation raster required by ArcGIS tools in this section are derived on the basis of the filled DEM.
218 Accordingly, the different drainage basin discretisation and network delineations are identified in relation to
219 the rainfall's spatial variation based on VRSS (the comparison test regarding network generations between the
220 sub-model approach and Arc-Malstrøm are provided in Supplementary Document S2).

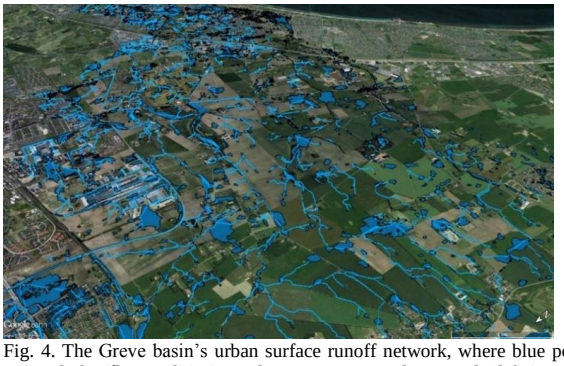

221
222 Fig. 4. The Greve basin's urban surface runoff network, where blue polygons represent blue spots (sinks) and blue lines represent
223 stream links (flow paths). (Map data: © 2017 Google, Digital Globe)

224 **2.3 Link-based fast-inundation spreading (Module III)**

225 In order to quickly estimate flood volumes across the basin-wise network, we developed a link-based fast-
226 inundation spreading algorithm (Fig. 2b). First it should be noted that, as seen from Eq. (2), rainfall-runoff
227 conversion on catchments is assumed as 100%. Given a specific modelling purpose – identifying simple

https://doi.org/10.5194/hess-2020-243
Preprint. Discussion started: 30 July 2020


Hydrology and Earth System Sciences
Discussions

228 Boolean flow conditions (spill-over/non-spill-over), the spatially-varying magnitude of rainfalls and the
229 complexity of terrains are considered as dominant factors affecting overland flow in case of large-scale
230 inundation. Therefore, detailed hydrological losses (i.e. evaporation and infiltration) and the presence of
231 underground drainage systems are deliberately disregarded to obtain the minimum computational efforts
232 exclusively accounting for the minimum necessary representation process.

233 The suggested algorithm uses stream links as computational objects. Therefore, all computational information
234 related to sink features (points), i.e. $C_{sink,\,Aggr}$, $V_{runoff}$, $V_{received}$, $V_{spilled}$ and $V_{remaining}$, is joined onto their intersected
235 stream links (edges). This allows for the subsequent fast-inundation calculation to be exclusively based on one
236 stream link feature class' attribute table (see Fig. 5b). The Shreve stream order (Shreve, 1966) is used to
237 determine the correct computational order of stream links and the convergence order of excess flows. By
238 governing the conservation of mass balance within each stream link, flood volumes are computed according
239 to two flow conditions:

240 If $V_{received} + V_{runoff} > C_{sink,\,Aggr.}$ (Flow condition I)

241 $$V_{spilled} = V_{runoff} + V_{received} - C_{sink,\,Aggr.} \quad (5)$$

242 $$V_{remaining} = C_{sink,\,Aggr.} \quad (6)$$

243 Else $V_{received} + V_{runoff} \leq C_{sink,\,Aggr.}$ (Flow condition II)

244 $$V_{spilled} = 0 \quad (7)$$

245 $$V_{remaining} = V_{received} + V_{runoff} \quad (8)$$

246 where $V_{spilled}$ represents excess volumes once the spill-over level is reached and $V_{remaining}$ is the actual volume
247 retained locally, and $V_{received}$ represents the converged flow volumes received from upstream connecting links.
248 $C_{sink,\,Aggr.}$ is obtained from Section 2.1. After enabling this algorithm, a stream link feature class incorporating

https://doi.org/10.5194/hess-2020-243
Preprint. Discussion started: 30 July 2020


Hydrology and Earth System Sciences
Discussions
Open Access
EGU

geometric features and their associated attribute table is produced (Fig. 5a and b). Notably, in addition to the computed results of $V_{spilled}$ and $V_{remaining}$, topological connectivity identifying the next downstream stream link is also self-established in the same table (upstream & downstream sink ID, see Fig. 5b), which is now ready for the upstream tracing operation as illustrated in Fig. 5c and explained further in Section 2.4.

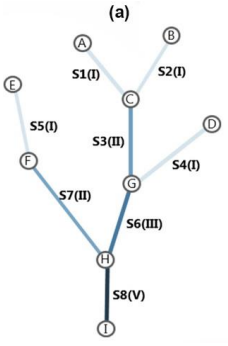


(b)

Attribute table

| StreamLinks ID | Shreve order | Sink ID (upstream) | $V_{runoff}$ ($m^3$) | $V_{received}$ ($m^3$) | $C_{sink,Aggr}$ ($m^3$) | $V_{spilled}$ ($m^3$) | $V_{remaining}$ ($m^3$) | Sink ID (downstream) | spill-over/ non-spill-over |
|---|---|---|---|---|---|---|---|---|---|
| S1 | I | A | 20 | 0 | 5 | 15 | 5 | C | YES |
| S2 | I | B | 30 | 0 | 30 | 0 | 30 | C | NO |
| S3 | II | C | 50 | 15 | 40 | 25 | 40 | G | YES |
| S4 | I | D | 100 | 0 | 90 | 10 | 90 | G | YES |
| S5 | I | E | 120 | 0 | 100 | 20 | 100 | F | NO |
| S6 | III | G | 400 | 35 | 200 | 235 | 200 | H | YES |
| S7 | II | F | 400 | 20 | 2000 | 0 | 420 | H | NO |
| S8 | V | H | 500 | 235 | 150 | 585 | 150 | I | YES |

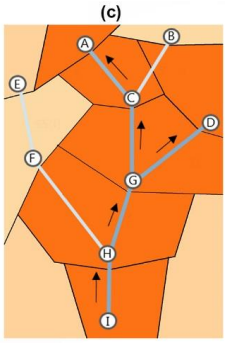


Fig. 5 (a) The geometric features of the stream link feature class, where points represent sinks with IDs (A–I), and edges representing their assigned stream links (S1–S8); the gradually darker blue colour symbolized the increase in Shreve stream order (I–V), which determines the computing sequence of stream links; (b) The stream link feature class' attribute table where the computational information is constructed by joining two points onto one stream link based on their spatial intersection (i.e. points A and C are the endpoints of edge S1). Blue rows mark the stream links with spill-overs, as determined from their associated geometric features shown to the right; (c) Sub-impact zones screening process, illustrated for target sink I. Black arrows represent tracing directions when searching for connected upstream stream links and the number of stream link features involved (S8 – S6 – S3 – S1 and S8 – S6 – S4) intuitively reflecting tracing distances. Dark orange areas symbolized identified sub-impact zones to be included while light orange areas symbolized eliminated sub-impact zones identified as irrelevant to target objects (Sink I).

Whereas a fast-inundation computation was presented by Balstrøm and Crawford (2018) previously, the essential difference of these two algorithms comes at the different approaches configuring the data structures for computations. Arc-Malstrøm's data structure is built on ArcGIS' geometric networks (Esri, 2019). The computational information (i.e. $C_{sink,\ Aggr}$, $V_{received}$, $V_{runoff}$, $V_{spilled}$ and $V_{remaining}$) is coded in the point (junction) class's attribute table, and the topological connectivity (e.g. points-to-points) are identified in a separate table (i.e. geometric network's relation class) during the set-up of ArcGIS's geometric network. Thus, this data structure formulates a point-based fast-inundation routing, where the mass conservation is computed exclusively based on the point class objects and the computing order is referred by the points-to-points relationship in the geometric network's relation class. In contrast, this new algorithm self-establishes the data structure that configures computational information as well as the self-identified topological connectivity into the stream link feature class' attribute table thus facilitating efficient data storage and retrieval from one source. More importantly, unlike Arc-Malstrøm's accessing the geometric network's internal function and class

https://doi.org/10.5194/hess-2020-243
Preprint. Discussion started: 30 July 2020


Hydrology and Earth System Sciences
Discussions

objects via the ArcObjects SDK, this new algorithm is programmed based on ArcGIS' Python interface (ArcPy) only, which facilitates the automation and wrap-up of all modules in a consistent programming environment.

### 2.4 Sub-impact zones screening (Module IV)

With the aim of identifying the relevant sub-impact zones, a screening algorithm is programmed to perform upstream tracing tasks based on the stream link feature class (Section 2.3). As suggested by Fig. 2c, when introducing the target objects among urban infrastructures (i.e. buildings, parks and roads) as input variables, the intersecting stream link features are first selected (i.e. S8 as it intersects with Sink I) representing local inundations as well as their associated inflow paths. Here, although spill-overs - due to the possible high-momentum flows - may impact all the neighbourhood flow conditions, their significant volumes would follow the preferential paths indicated by stream links, thus affecting the downstream flow conditions primarily. Meanwhile, a sink could receive multiple inflows. To fully expose multiple inflow paths, the procedure continuously matches all the stream links by indexing the current upstream sink ID until all the upstream stream links being identical downstream sink ID were included (Fig. 5b). More importantly, in order to reflect the actual flow continuity beyond flow paths (simply indicating flow directions), flood volumes along the stream links are taken into account by conserving the mass balance during the whole tracing procedure. Here, based on $V_{spilled}$, we introduce a Boolean flow condition property (spill-over/non-spill-over, see Fig. 5b) as a search termination criterion. So, stream links associated with non-spilled-over sinks (i.e. tracing-brake features) are excluded from the search list, which results in optimal stream links (i.e. S8-S6-S3-S1 or S8-S6-S4, see Fig. 5c). In case of heavy rainfall, the tracing distance would increase with more involved stream links due to the more densified spilling configurations and vice versa (Fig. 6). This thereby avoids a substantial risk of tracing all connected flow paths basin-wise, such as Arc-Malstrøm's upstream tracing function and ArcGIS' Watershed tool. Finally, since these identified stream links represent all main flows related to specified inundation modelling, their intersected sub-impact zones would suggest suitable modelling areas (domains) covering relevant runoff generations (sheet-flow) as well as flood propagations (channel-flow).

https://doi.org/10.5194/hess-2020-243
Preprint. Discussion started: 30 July 2020


Hydrology and Earth System Sciences
Discussions
Open Access
EGU

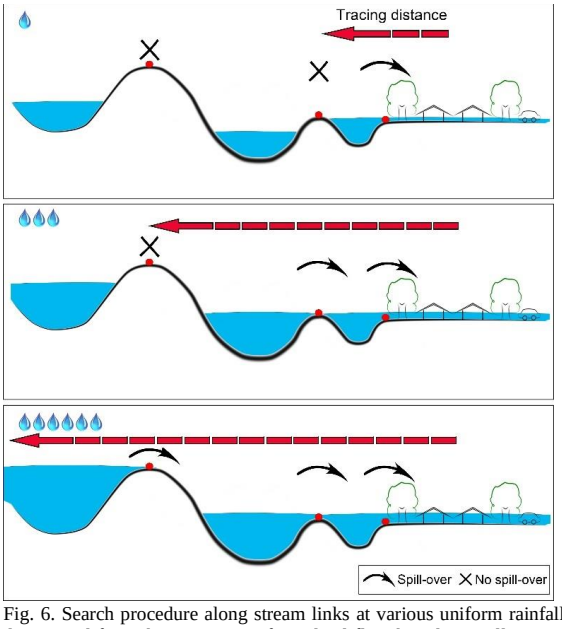


Fig. 6. Search procedure along stream links at various uniform rainfall scenarios, where the optimal tracing distance (red arrow) is determined from the continuity of overland flow based on spill-over and non-spill-over properties. Note: The number of raindrops (blue) represents the rainfall's magnitude and No spill-over refers to the termination criterion to stop further upstream tracing. In case of distributed rainfall, various optimal tracing distance in relation to target objects should be determined.

### 2.5 Tailor-made sub-model generation (Module V)

Urban flow is usually characterised by numerous transitions of supercritical flows and numerical shocks (Hunter et al., 2008). Full 2D models are considered as best candidates to expose the complicated flow dynamics. Thus, MIKE FLOOD's rectangular cell solver, which solves alternating direction implicit schemes on inertia wave equations (ADI), is used in this module to obtain dynamic 2D flow predictions (DHI Water & Environment, 2017). More importantly, by accounting for identified sub-impact zones, critical computational grid-cells (dark orange cells) intersecting them are extracted from the high-resolution DEM's grid. Thus, a reduced modelling grid extent is identified simultaneously, resulting in efficient computational costs for MIKE FLOOD's 2D simulations, see Fig. 7a. Besides, the suggested 1D flow patterns (blue edges) define that runoffs generated within the identified sub-impact zones must exit at downstream terminal pour points (i.e. Sink I's pour point), only. To be consistent with these described 1D flow conditions, the irrelevant grid-cells (light orange cells) within the reduced modelling grid extent should be assigned the Nodata value to prevent outwards 2D flow leakages along the upstream edges. 2D weirs should be established by pulling up the terminal pour

https://doi.org/10.5194/hess-2020-243
Preprint. Discussion started: 30 July 2020


Hydrology and Earth System Sciences
Discussions

point's surrounding elevation values (marked ↓ in Fig. 7b) to the spilling level, while sufficient retention volumes > $V_{spilled}$ should be accommodated to the downstream side of the 2D weirs by decreasing the associated grid-cell elevations (marked × in Fig. 7b). For the grid-cells intersecting the internal subtracted areas or buildings, their elevation values should be substituted by a specified value (e.g. 100) to be excluded from the final 2D flow computations. Based on the reduced domain (dark orange cells) and the optimised boundary conditions (the red outline) determined above, additional complexities (e.g. hydrological losses, distributed roughness surface values, impervious surface types and hydraulic behaviours concerning rooftops) may be involved subsequently at the local catchment scale. Thus, this GIS-based method ultimately produces tailor-made sub-models providing fast 2D flow predictions.

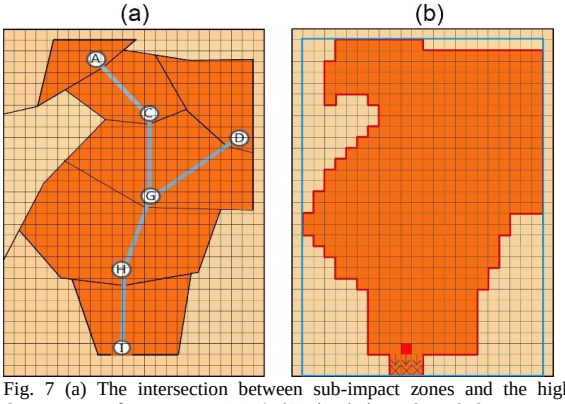


Fig. 7 (a) The intersection between sub-impact zones and the high-resolution DEM's grids; (b) The computational domain determination for MIKE FLOOD's 2D simulation, where dark orange grid-cells represents critical computational cells configuring the reduced computational domain, the blue frame represents the reduced rectangular modelling grid extent and the red frame represents the reduced computational domain and the optimised boundary conditions. The red grid-cell represents the location of terminal pour points, and the grid-cells marked ↓ configure the 2D weir having the spilling elevation level. Furthermore, the grid-cells marked × configure retention volumes based on decreased elevations.

### 2.6 Model experiments

The sub-model approach suggests two outcomes: i) reduced computational domains and ii) optimised boundary conditions. To clarify the individual effect, their validities were investigated separately as two-folds: On one hand, the suggested domains can lead to fast 2D predictions in MIKE FLOOD. Yet, their prediction accuracy may be affected as well. To quantify the influence of domain reductions, tests using consistent boundary conditions were conducted to validate this method against benchmark results, and the other domain reduction approach (Municipality domain approach, Section 2.6.1) was used for comparison purposes. On the

https://doi.org/10.5194/hess-2020-243
Preprint. Discussion started: 30 July 2020


Hydrology and Earth System Sciences
Discussions

other hand, optimised boundary conditions may lead to prediction discrepancies along the boundary areas. To evaluate the influence of the various boundary conditions adopted, tests using the consistent domain were conducted to compare benchmarking discrepancies in different boundary conditions. Furthermore, as according to Leitão et al. (2009) different types of terrain morphology may impact overland flow patterns significantly, tests (Section 2.6.3) were carried out on different catchments (within the Greve basin described in Section 3.1) under different associated regional rainfalls (Section 3.2) to validate the general applicability and the robustness of the sub-model approach.

**2.6.1 Domain reduction tests (sub-model approach vs. municipality domain approach)**

We identified the full-basin domain approach, where the entire drainage basin area has flow directions pointing towards the outlet (i.e. ArcGIS' Basin/Watershed tool). Further, this approach converts the whole area into the full 2D domain in the MIKE FLOOD (Fig. 10a). As we enable 2D dynamic flows at the full-basin domain, this approach reproduced the most accurate flow dynamics thus taken as the benchmark solution. Yet, without having any specified targets, this approach reflects general modelling targets. In contrast, taking the buildings within focus area A as the specific target objects (Map A, Fig. 8), we identified two different reduced domains following two approaches: i) the sub-model approach, where the sub-model domain (Fig. 10b) was delineated as the suggested approach; ii) the municipality domain approach, where a reduced domain was delineated simply based on municipality borders including all target objects (Fig. 10c).

In order to ensure the consistent starting point for comparisons, the same inputs – i.e. DEMs Section 3.2 and Rainfall Section 3.3 – were used for the three approaches. Yet, due to the different domains determined from the different approaches, the two inputs for the sub-model approach and the municipality domain approach were tailored by having a mask operation (i.e. ArcGIS' Extract by Mask tool) based on their suggested domain, respectively. Finally, the predictions of the sub-model approach and the municipality domain approach were both validated against the benchmark solution within the same extents of the masks, and discrepancies of the two approaches were further compared regarding flood extents, flood depths internal points' hydrographs and computational efficiencies. In this test, to exclude the influence of the inconsistent boundary conditions,

https://doi.org/10.5194/hess-2020-243
Preprint. Discussion started: 30 July 2020


Hydrology and Earth System Sciences
Discussions

366 uniform closed-boundary conditions were adopted for all three approaches (the test based on uniform open-
367 boundary conditions are provided in Supplementary Document S4).

368 **2.6.2 Boundary condition comparison tests (optimised boundary conditions vs. uniform closed-**
369 **boundary conditions vs. uniform open-boundary conditions)**

370 We identified the optimised boundary conditions as suggested by the sub-model approach. With the same sub-
371 model domain, the simulations based on uniform closed-boundary conditions and the uniform open-boundary
372 conditions were carried out for comparison purposes. Like Section 2.6.1, the same rainfall input was used for
373 the three approaches. All these results were validated against the benchmark solution within the same extent
374 of the sub-model domain respectively, and their discrepancies were compared regarding flood extents and
375 flood depths. Finally, the internal points that illustrated significant discrepancies in hydrographs (Section 2.6.1)
376 were investigated further.

377 **2.6.3 General applicability tests (Sub-model A vs. B vs. C vs. D)**

378 We selected four focus areas (Map A, B, C and D, Fig. 8) representing various typical topographies from the
379 three regions described in Section 3.1, and buildings (orange polygons in Map A, B, C and D) were in turn
380 listed as specified target objects. Four sub-models and their predictions were generated by targeting different
381 flooded objects as well as their associated rainfalls representing return periods of 1-100 years (detailed rainfall
382 inputs were provided in Supplementary Document S5). Likewise, the benchmark solution was used to validate
383 their discrepancies within the same extents of the four sub-models' domains. To pursue the most accurate sub-
384 model predictions, their identified optimised boundary conditions were adopted in this test.

385 **3. Case-studies**

386 **3.1 Study site**

387 The study area is "the Greve basin" located on Zealand, Denmark, approximately 30 km SW of Copenhagen,
388 that includes both rural and urban areas. The study basin's extent of 73.8 $km^2$ was determined from a Danish
389 nationwide hydrologic conditioned elevation model (DHyM) using ArcGIS' Basin tool. With reference to Fig.
390 8, the eastern urbanised region's terrain (dark orange) is low-lying and flat (Avg. elevation of 3.81 m with St.

https://doi.org/10.5194/hess-2020-243
Preprint. Discussion started: 30 July 2020


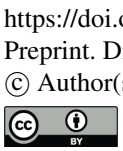

Hydrology and Earth System Sciences
Discussions
Open Access
EGU

391 dev. of 1.85 m), the central region (light orange) is slightly undulating (Avg. elevation of 14.74 m with St. dev.
392 of 5.44 m) while the westernmost region (yellow to green) is the highest-lying with the steepest gradients
393 within the basin (Avg. elevation of 37.4 m with St. dev. of 8.84 m). Thus, the basin's topography demonstrates
394 complications regarding the spatial variation of terrains. In addition, a receptor waterbody (blue polygon, Fig.
395 8) representing sea level elevation is located towards east/southeast acting as the basin's outlet collecting all
396 runoffs.

397

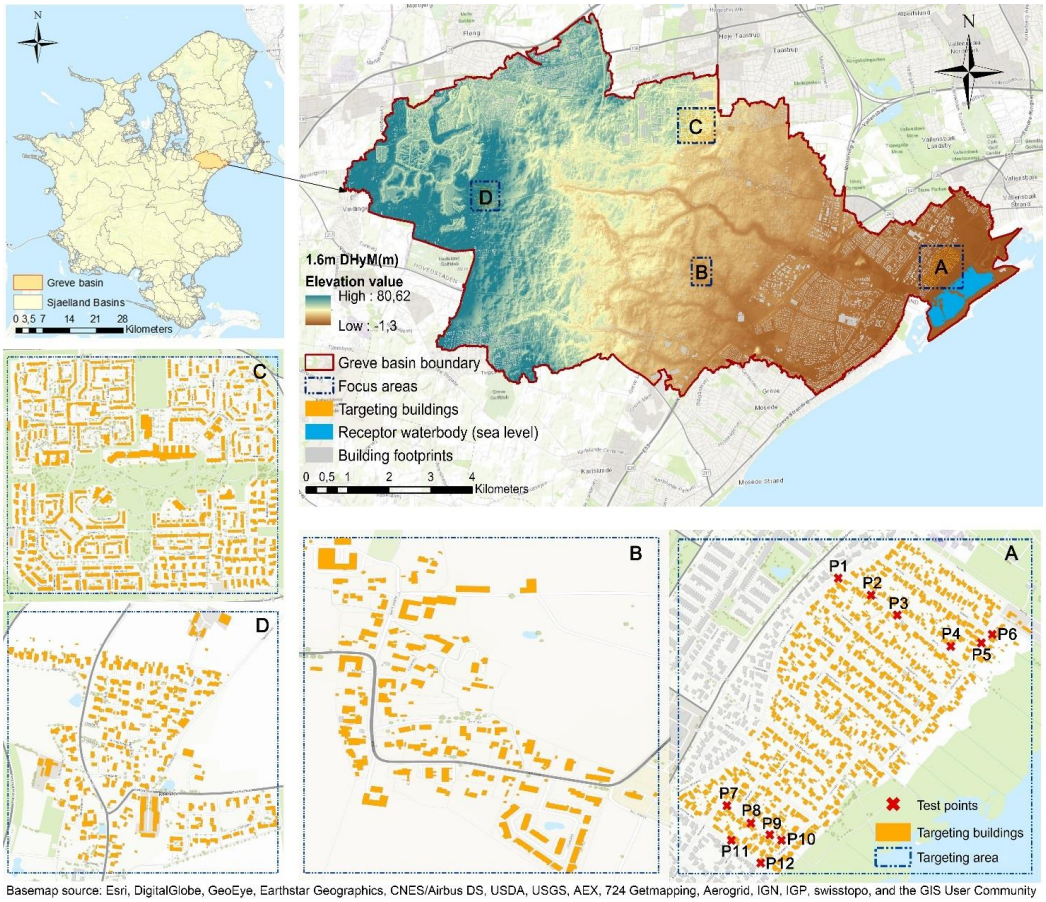


398 Basemap source: Esri, DigitalGlobe, GeoEye, Earthstar Geographics, CNES/Airbus DS, USDA, USGS, AEX, 724 Getmapping, Aerogrid, IGN, IGP, swisstopo, and the GIS User Community
399 Fig. 8. Case study area: Basin divisions for Zealand and location of the Greve basin (upper left); the hydrologically conditioned
400 elevation model (1.6 m resolution) covering the Greve basin (upper right). Map A, B, C, and D show four selected focus areas and
401 their target objects (buildings) that were hit by the extreme rainfall event on July 2nd, 2011. Areas marked with a red X represent
402 locations where water depths and velocity hydrographs are extracted (L-shaped in the northeast, F-shaped in the south).

403

https://doi.org/10.5194/hess-2020-243
Preprint. Discussion started: 30 July 2020


Hydrology and Earth System Sciences
Discussions

### 3.2 Input DEMs and pre-processing enhancements

The generation of the urban surface runoff network (Section 2.2) benefits from the quality of the DEM regarding grid size, data accuracy (horizontal/vertical), DEM generation technologies and data sources (Adeyemo et al., 2008; Leitão et al., 2009; Leitão, 2016). To avoid massive computational expenses while incorporating sufficient precision to reflect micro-topographies such as road curbs, the DHyM with a resolution of 1.6 m and a vertical accuracy of 0.05 m was selected (Data Supply and Efficiency Board, 2013). However, since this DHyM excludes roof elevations and contains ground elevations only, an urban surface runoff network analysis based exclusively on a DHyM may lead to miss-reflections of localised floods and an underestimation of total sink volumes (Jensen et al., 2010; Leitão et al., 2009). If instead, a Digital Surface Model (DSM) is used, this may include noises from, for example, tree canopies and parked cars. Sensitive to these issues, building elevations from a DSM was fused with the DHyM, thus obtaining a "combined" DEM as input to the sub-model approach.

### 3.3 Rainfall

An extreme precipitation event on July 2nd, 2011 was selected. Due to the large extent of the Greve basin, we used data from five available rain gauges to cover the basin-wise rainfall heterogeneities (see Fig. 9). The Thiessen polygon approach was applied to distribute precipitation data from these rain gauges onto their nearest neighbourhoods (Fig. 9), simulating the pattern of the progressively decreasing rainfall from the eastern coastline towards western inland. According to the time-series of I5805 (shown as hyetographs in Fig. 9), the overall simulation time of 172 minutes was used for MIKE FLOOD, where the simulation continued for 97 minutes after the main peak, allowing for the sufficient time for flood peaks to flow through the landscape.

https://doi.org/10.5194/hess-2020-243
Preprint. Discussion started: 30 July 2020


Hydrology and Earth System Sciences
Discussions

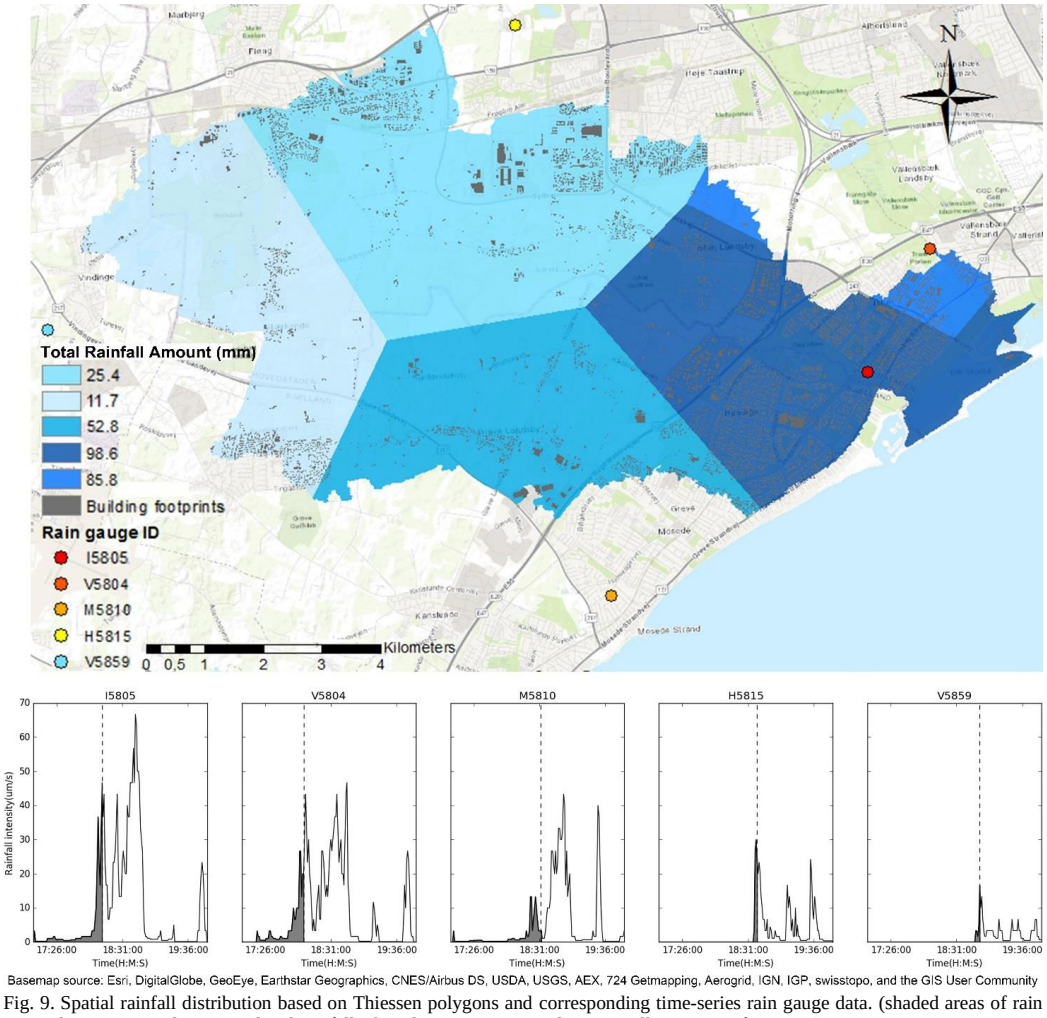


Basemap source: Esri, DigitalGlobe, GeoEye, Earthstar Geographics, CNES/Airbus DS, USDA, USGS, AEX, 724 Getmapping, Aerogrid, IGN, IGP, swisstopo, and the GIS User Community

Fig. 9. Spatial rainfall distribution based on Thiessen polygons and corresponding time-series rain gauge data. (shaded areas of rain gauge data represent the accumulated rainfall when the unimportant sinks start spilling over in five areas)

### 3.4 Modelling parameters

The $HRV_{ratio}$ parameter was set to 15%, considering that the corresponding accumulated rainfall (i.e. 14.8 mm = 15% × 98.6 mm, gauge I5805) is relatively small compared to the total. Next, a $VL_{ratio}$ of 5% was applied to decide upon the final removal of $VL_{Aggr}$. For the MIKE FLOOD computations, default parameters were used for the 2D engine (DHI Water & Environment, 2017). A uniform surface friction value (Manning Roughness Coefficient, M = 32) was assumed, and a dry surface was defined as the initial condition. In case of the insignificant influence of evaporation and infiltration and drainage systems during the rainfall event, the 100%

https://doi.org/10.5194/hess-2020-243
Preprint. Discussion started: 30 July 2020


Hydrology and Earth System Sciences
Discussions
Open Access
EGU

434 rainfall-runoff conversion was assumed, and drainage systems were excluded for MIKE FLOOD's 2D flow
435 computations.

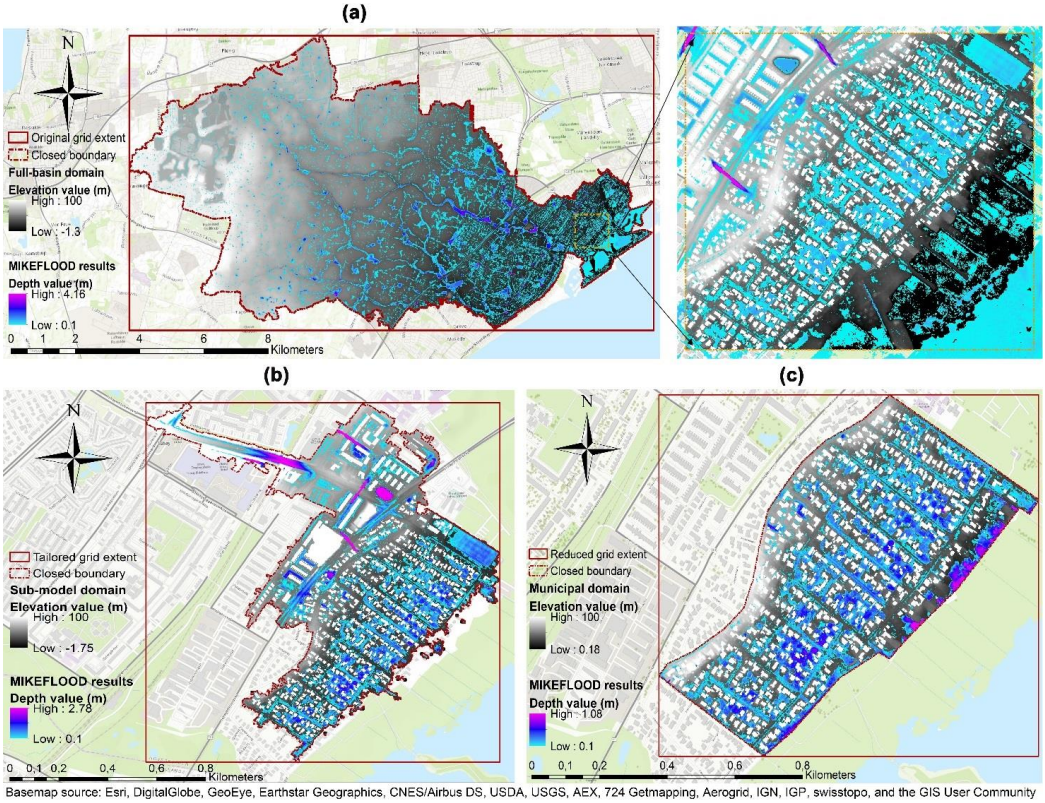


436
437 Fig. 10. 2D flow domains determined by three approaches and their associated predictions based on MIKE FLOOD: (a) The full-basin
438 domain determined from the full-basin high-resolution DEM. Notably, since the downstream receptor water body is involved as one
439 part of the computation domains to collect the basin runoffs, the predictions on land areas can be considered as benchmark results,
440 whereas the uniform closed boundary was adopted; (b) The sub-model domain, where the sub-model approach delineates the reduced
441 domain accounting for the basin-wise 1D static flows; (c) The municipality domain determined from municipality borders. The red
442 frame represents the extent of 2D model grids, the dotted frame defines the external modelling boundary, and the transparent spaces
443 in-between two frames define the Nodata grid-cells. The grid-cells with the value of 100 define the excluded internal domain (i.e.
444 buildings and non-spilling sub-impact zones) in MIKE FLOOD. Note: The figure on the right side of Fig. 10a shows benchmark results
445 zoomed in the same extent as the other approaches for easy comparisons.

446 **4. Results**

447 **4.1 Domain reduction tests**

448 **4.1.1 Maximum depth flood extent**

449 MIKE FLOOD's 2D prediction results produced from the three different domains are presented in Fig. 10a, b
450 and c, where a 10 cm flood depth was adopted as the threshold defining critical flood depths. To demonstrate

https://doi.org/10.5194/hess-2020-243
Preprint. Discussion started: 30 July 2020


Hydrology and Earth System Sciences
Discussions

the discrepancies of maximum depth flood extents, binary analyses (dry/wet) from the status of the flooded cells were conducted (Fig. 11a and b). The predicted inundation extents were in good agreement in most areas, while overestimations occurred along the downstream edge as expected from using the closed boundary. In contrast to the municipality domain approach, the sub-model approach returned fewer overestimations that tended to occur near terminal pour points only.

The critical depth threshold value may affect the flood extent significantly. To fully expose the flood extent discrepancies of the two approaches, their results were further compared using different threshold values, adopting the $F^2$ statistic (Werner et al., 2005) as a performance indicator. In Table 1, high goodness of fit above 0.86 was observed in both approaches for either a depth threshold of 0.01 m or 0.05 m. However, following progressive increases of the threshold value, the sub-model approach showed a robust performance on flood extent predictions with $F^2$ values > 0.91, while the $F^2$ value for the municipality domain approach started to drop sharply at the value of 0.15 m, indicating significant errors.

**Table 1**

$F^2$ values for the sub-model approach vs. the municipality domain approach.

| Depth threshold (m) | 0.01 | 0.05 | 0.1 | 0.15 | 0.2 | 0.25 | 0.3 | 0.35 | 0.4 |
|---|---|---|---|---|---|---|---|---|---|
| **Sub-model approach $F^2$** | 0.970 | 0.956 | 0.941 | 0.928 | 0.923 | 0.917 | 0.913 | 0.914 | 0.911 |
| **Municipality domain approach $F^2$** | 0.913 | 0.861 | 0.808 | 0.765 | 0.734 | 0.689 | 0.603 | 0.504 | 0.323 |

https://doi.org/10.5194/hess-2020-243
Preprint. Discussion started: 30 July 2020


Hydrology and Earth System Sciences
Discussions
Open Access
EGU

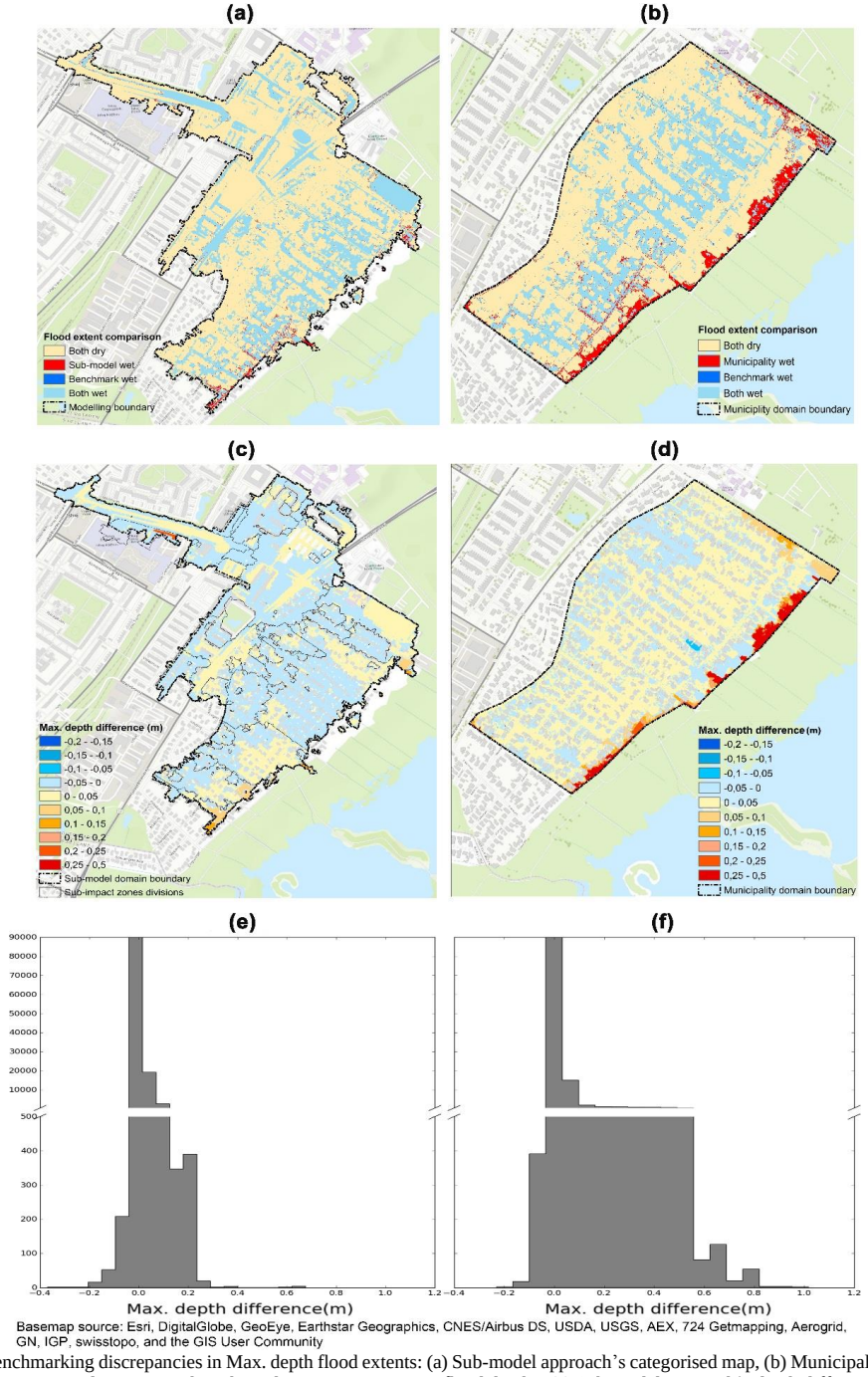


Fig. 11. Benchmarking discrepancies in Max. depth flood extents: (a) Sub-model approach's categorised map, (b) Municipality domain approach's categorised maps. Benchmarking discrepancies in Max. flood depths: (c) Sub-model approach's depth difference map, (d) Municipality domain approach's depth difference map, (e) Sub-model approach's histogram of Max. depth difference, (f) Municipality domain approach's histogram of Max. depth difference.

https://doi.org/10.5194/hess-2020-243
Preprint. Discussion started: 30 July 2020


Hydrology and Earth System Sciences
Discussions

#### 4.1.2 Maximum flood depth

Fig. 11c and d show the spatial distribution of the maximum flood depth differences (subtracting benchmark results from the sub-model domain's predictions and the municipality domain's predictions). Discrepancies of $\pm$ 0.05 m were seen in majority areas of the sub-model domains. Interesting, most underestimations of $-$ 0.05 m were found to the upstream side of the sub-impact zones for the sub-model approach. This may be explained by the "8N approach" adopted when determining flow directions, where runoff is forced into one direction of eight adjacent cells. Thus, based on this "confined flow" algorithm, each sub-impact zone delineated was considered as the minimum contributing area only. If we refer to the flow direction along the steepest gradient as the major runoff (being fully harvested) and other directions as minor runoff, then the minor runoff, especially along defined upstream boundaries, may be miss-captured. Nevertheless, discrepancies of < 0.05 m, compared to the vertical accuracy of the DEMs used, is considered insignificant. Close to the downstream boundary of the municipality domain, regional overestimations were observed in maximum flood depths. Because the closed boundary pulled up the spilling level limitlessly, the maximum differences > 1 m may be considered as problematic deviations from the benchmark. Notably, those red pixels indicating the highest flow accumulations suggest shifted terminal pour point positions as opposed to the sub-model approach. Apparently, for these positions, the sub-model approach produced significantly fewer over-predictions for the downstream boundary than did the municipality domain approach.

The histograms of maximum depth differences are displayed in Fig. 11e and f. A higher frequency of over-predictions occurred for the municipality domain approach's histogram, while a near-symmetric distribution of over- and under-predictions, approximately similar to the normal error distribution, was identified for the sub-model approach. The statistics for the maximum flood depth difference for both approaches were summarised in Table 2. Root Mean Square Errors (RMSE) of 0.02 m for the sub-model approach in the overall domain were below the vertical accuracy of the DEM. Also, to validate prediction discrepancies adjacent to targeted buildings, a targeting section was delineated by creating a buffer (3.2 m, the width of two grid cells) around them. In targeting sections, marginal discrepancies were observed both in benchmarking comparisons

https://doi.org/10.5194/hess-2020-243
Preprint. Discussion started: 30 July 2020


Hydrology and Earth System Sciences
Discussions

and in comparisons of the two approaches. This is possibly due to the location of the buildings that is far away from impact areas caused by the backwater effect.

**Table 2**

Statistics of flood maximum depth difference for the sub-model approach vs. the municipality domain approach.

| | Overall domain | | | | Targeting section | | | |
|---|---|---|---|---|---|---|---|---|
| | **Minimum (m)** | **Maximum (m)** | **Mean (m)** | **RMSE (m)** | **Minimum (m)** | **Maximum (m)** | **Mean (m)** | **RMSE (m)** |
| **Sub-model approach** | -0.37 | 0.68 | 0.00 | 0.02 | -0.22 | 0.36 | 0.00 | 0.02 |
| **Municipality domain approach** | -0.23 | 1.02 | 0.02 | 0.08 | -0.23 | 0.43 | 0.01 | 0.02 |

### 4.1.3 Internal points depths and velocity hydrographs

To clarify discrepancies in spatial-temporal flow developments, hydrographs including water depths and flow velocity in u- and v-directions were extracted for the three approaches (Fig. 12a and b). Two runoff patterns each containing 6 points were selected as a simplified representation of runoff dynamics in the focus area A (see Fig. 8, Map A), referred to as an L- and F-shaped flow pattern. In the L-shaped flow pattern, the selected positions are characterised by either conveyance flooding or ponding flooding (Allitt et al., 2009). Hence, points 1, 3 and 5 identify areas where surface depressions result in permanent ponding, whereas convergent and high-velocity flows occur near points 2, 4 and 6. The F-shaped flow pattern is primarily characterised by localised ponding flooding. Point 7 denotes the concentration of flows that collects runoffs from its north-westerly regions. This concentrated flow proceeds towards the southeast and intrudes into depression zones at point 8. Yet, at this point, two branch currents split from the origin, where one flows over point 9 and terminates at point 10 as permanent ponding, while the other branch hits point 11 and further flows towards point 12 presenting ponding flooding in the southernmost corner.

Fig. 12a shows hydrographs for points 1–6 in terms of depths, u- and v-velocities for the L-shaped flow pattern. For points 1–5, good agreements with the benchmark regarding depths hydrograph's rising and falling limbs were obtained when using the sub-model approach. For points 1 and 2, in contrast to the municipality domain approach, average higher depth values accompanied by higher flow velocities for the sub-model approach were observed. Most likely, this happens because the extended regions restored the flooding propagation channel

https://doi.org/10.5194/hess-2020-243
Preprint. Discussion started: 30 July 2020


Hydrology and Earth System Sciences
Discussions

allowing more water outside the targeted region to enter, which is consistent with findings by Yu and Coulthard (2015). Additionally, whereas over-predictions occurred at the downstream ponding area of point 6, this error of < ~ 0.05 m was considered insignificant. Apparently, u- and v-velocity hydrographs derived from the sub-model approach mostly replicated the predictions in the benchmark at points 1–5. Yet, an entirely different flow direction was identified at point 6 compared to the benchmark, whereas minor differences of < 0.02 $ms^{-1}$ were found. As the consequence of the closed boundary, its hydraulic behaviour alters the actual runoff patterns, i.e. spilling to downstream, into a permanent ponding condition, and further inverse the flow direction due to the corresponding backwater effect.

Fig. 12b presents hydrographs of points 7–12 in terms of depths, u- and v-velocity for the F-shaped flow pattern. For points 7–9, overall goodness of fit with the benchmark was seen for the two approaches, suggesting marginal discrepancies of depths < ~ 0.05 m and velocities < ~ 0.03 $ms^{-1}$. In contrast, greater discrepancies of ~ 0.32 $ms^{-1}$ were identified for the u-velocity of point 10. Here, a southeast-directional flux was found for the municipality domain approach, while a permanent ponding suggested by near-zero flow velocities was seen for the sub-model approach. For points 11–12, depth overestimations of ~ 0.05m were shown in the sub-model approach for the sake of the closed boundary. Although the municipality domain approach presents similar results to the benchmark, it is worthwhile noticing that an opposite flow direction was found for the u-velocity. At this point, the sub-model approach reproduces a more precise flow pattern compared to the municipality domain approach. Notably, for points 6, 10 and 12, whereas an agreement was found for depth hydrographs of three approaches, substantial divergences in flow directions were identified, which illustrates higher sensitivity in u- and v-velocities towards the alternation of the flow patterns. Hence, instead of flow depths, we consider that u- and v-velocities are more sensitive indicator implying whether the desired flow patterns are reproduced precisely.

https://doi.org/10.5194/hess-2020-243
Preprint. Discussion started: 30 July 2020


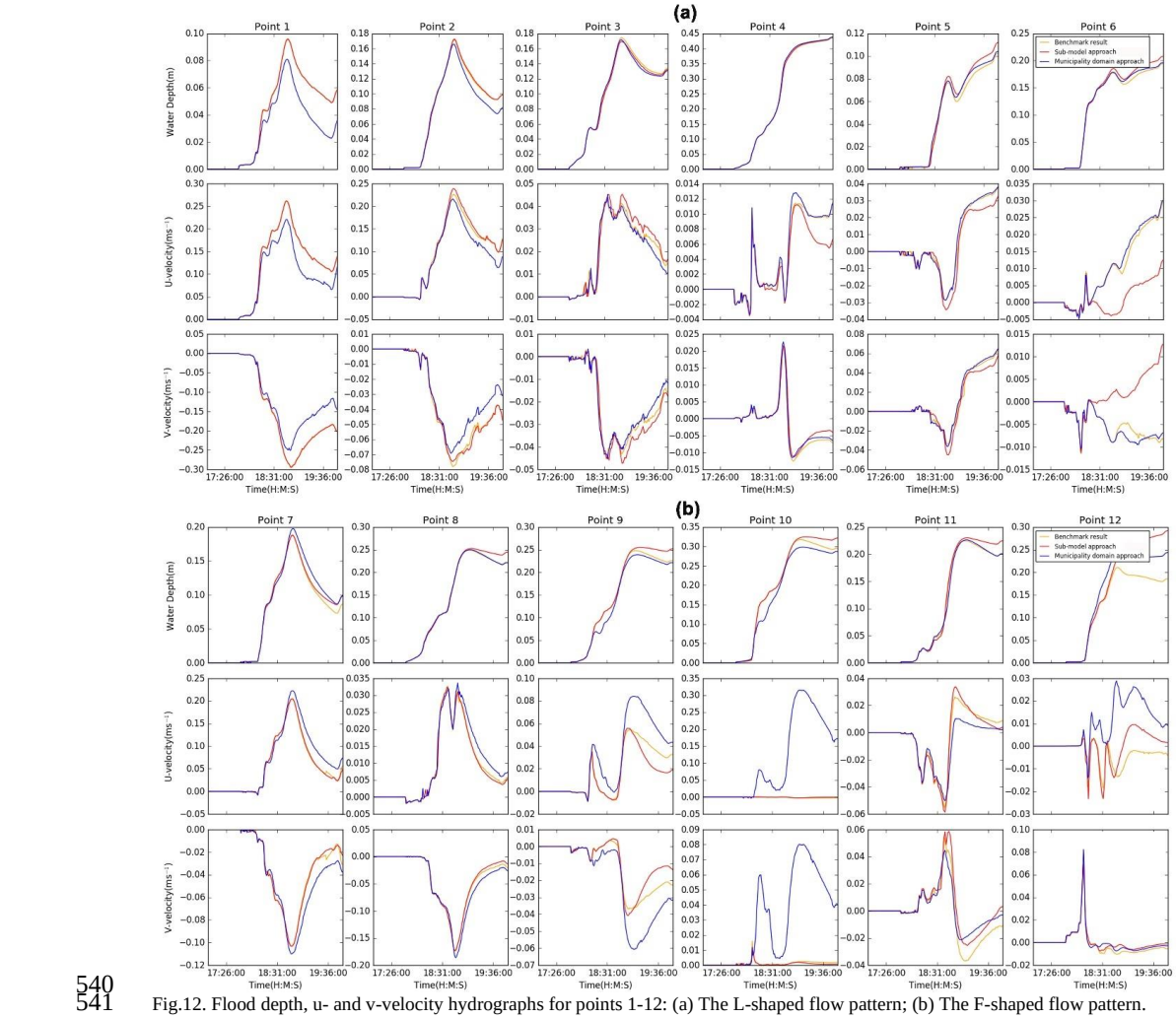


Fig.12. Flood depth, u- and v-velocity hydrographs for points 1-12: (a) The L-shaped flow pattern; (b) The F-shaped flow pattern.

### 4.1.4 Computational efficiencies

The sub-model approach was executed in ArcGIS Desktop ver. 10.6. Table 3 shows the computational time tested on a laptop computer (Intel®Core™ i7-5600 CPU @ 2.60GHZ, 8GB of RAM). Based on GIS processing environments, phase I (see Fig. 1) is grouped into raster (Module I and II) and vector processing modules (Module III and IV), and their operational independency are maintained in the general workflow. That means, although the costly computational time (e.g. 2,321 seconds) is required for the raster processing, once accomplished, the sub-impact zone tracing tasks could be processed quickly and repetitively in the vector

https://doi.org/10.5194/hess-2020-243
Preprint. Discussion started: 30 July 2020


Hydrology and Earth System Sciences
Discussions

549 processing environment, thus ensuring the fast generation of various sub-models when different target objects
550 were specified.

551 By applying the sub-model approach, 99% of the computational cells were excluded from the full-basin
552 domain for numeric computations of 2D flows, thus resulting in a factor 80 reduction with respect to elapsed
553 time (calculated from Table 3). Although the municipality domain approach also harvested time reductions,
554 prediction accuracy along the boundary areas was problematic due to the violation of the actual flow pattern
555 (Section 4.1.1, 4.1.2 and 4.1.3).

556 **Table 3**
557 Comparison of computational efficiency when using different domain approaches.

| | | Full-basin domain approach | Sub-model approach | Municipality domain approach |
|---|---|---|---|---|
| **Input DEM's grid extent (Columns × Rows)** | | 10202 × 5263 | 10202 × 5263 | 10202 × 5263 |
| **Tailored grid extent (Columns × Rows)** | | × | 903 × 967 | 701 × 612 |
| **Total No. of computational cells (wet)** | | 27,124,785 | 263,278 | 148,258 |
| **Pre-processing time (s) (Phase I)** | **Raster processing** | × | 2,321 | × |
| | **Vector processing** | × | 111 | × |
| **MIKE FLOOD simulation time (Phase II)** | **Elapsed time (s)** | 482,412 | 6,090 | 2,903 |
| | **CPU time (s)** | 1,141,666 | 24,330 | 11,585 |
| | **Time step (s)** | 0.2 | 0.2 | 0.2 |

558

559 **4.2 Boundary condition comparison tests**

560 Fig. 13 shows the benchmarking discrepancies in terms of flood extents, flood depths and points' hydrographs
561 when using different boundary conditions based on the same sub-model domain. In comparisons with three
562 boundary conditions, the optimised boundary condition suggested by the sub-model approach presents the
563 minimal predictions discrepancies of < ~0.5 m from the benchmark solution, particularly at the terminal pour
564 point position. This is because the adopted 2D weir restores the actual flow pattern and thus allows the spill-
565 over to take place at a constant elevation level. Further, other than the depth hydrographs, a goodness of fit
566 against the benchmark solution was identified in u- and v-velocities when using the optimised boundary
567 condition (Fig. 13g). As this stand, we conclude that the suggested algorithm resolves the overestimations in
568 Section 4.1 properly and yields the highest accuracy in flow dynamics along the boundary areas. Yet, when

https://doi.org/10.5194/hess-2020-243
Preprint. Discussion started: 30 July 2020


Hydrology and Earth System Sciences
Discussions
Open Access
EGU

569 the uniform open-boundary condition was used, significant underestimations in maximum flood extents and
570 flood depths were seen along the edges of the sub-model domain, where unrealistic 2D flow leakages were
571 identified due to the lowered spilling level. As such, we consider the open-boundary condition inappropriate
572 since the 2D flows derived is inconsistent to the predefined 1D runoff conditions.

https://doi.org/10.5194/hess-2020-243
Preprint. Discussion started: 30 July 2020


Hydrology and Earth System Sciences
Discussions

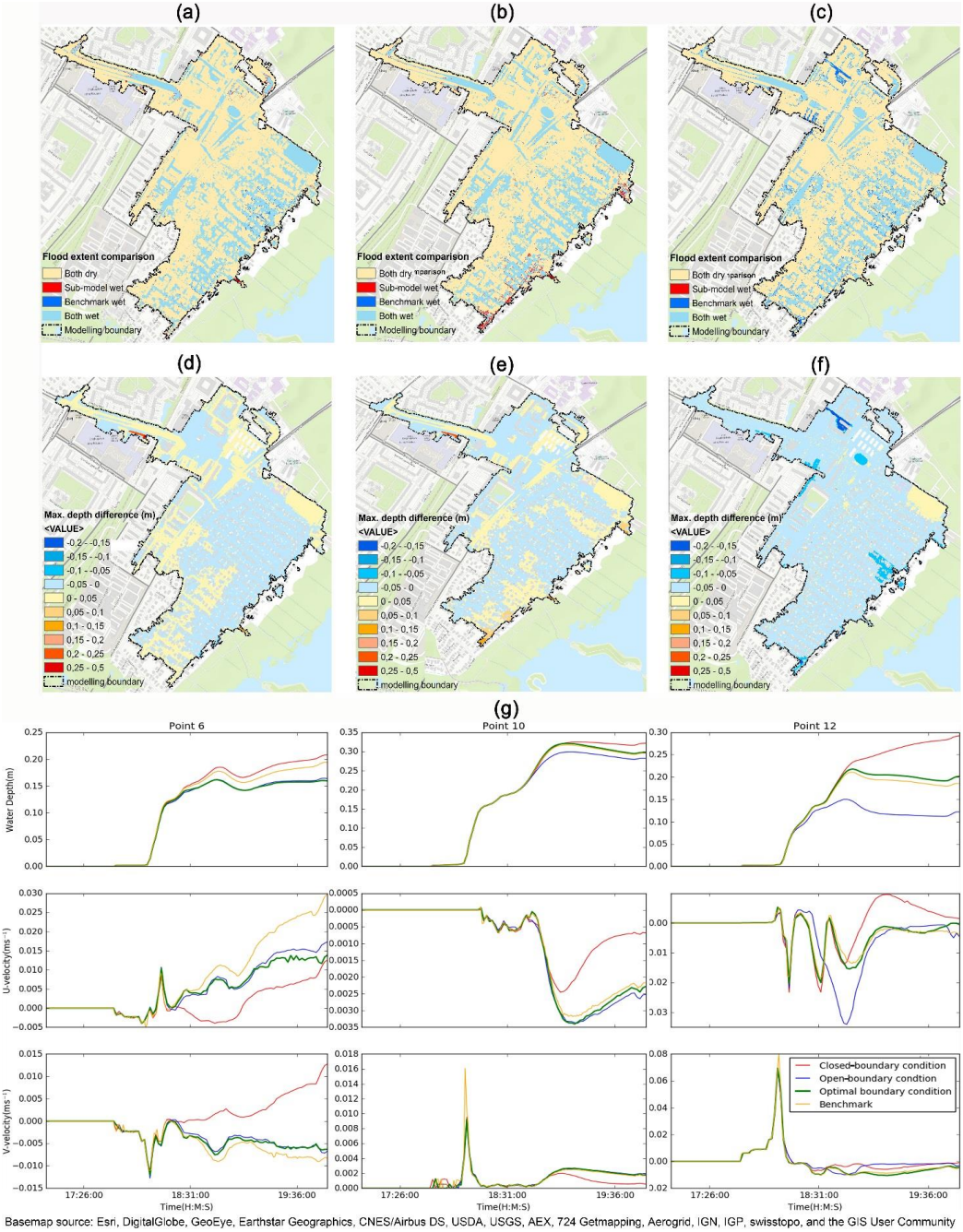


Fig.13 Benchmarking discrepancies using different boundary condition strategies: (a) The optimised boundary condition's flood extent categorised map, (b) The uniform closed-boundary condition's flood extent categorised map, (c) The uniform open-boundary condition's flood depth difference map, (d) The optimised boundary condition's flood depth difference map, (e) The uniform closed-boundary condition's flood depth difference map, (f) The uniform open-boundary condition's flood depth difference map; (g) Flood depth, u- and v-velocity hydrographs for points 6, 10 and 12 using the different boundary conditions.

https://doi.org/10.5194/hess-2020-243
Preprint. Discussion started: 30 July 2020


Hydrology and Earth System Sciences
Discussions

### 4.3 General applicability tests

Fig. 14 shows the outputs of four different sub-models (Sub-model A, B, C and D) in terms of 1D flow conditions, identified computational domains and corresponding MIKE FLOOD's 2D predictions. In accordance with Section 2.4, longer return period rainfalls resulted in longer maximum tracing distances. However, in response to the 50-year return period rainfall, Sub-model B identified the longest tracing distance of 2,535 m as well as the highest maximum spill-over volumes of 43,945 $m^3$. The reason for this exception is due to its special catchment topographies, where only one flood propagation channel was identified discharging the substantial runoffs accumulated from the largest catchment area of 1,676,207 $m^2$. Conversely, as the result of substantial tracing-brake features identified during shorter return period rainfalls, scattered independent areas suggesting localised flooding phenomenon were found in the southern part of Sub-model C and the northern part of Sub-model D. As for 2D flow prediction accuracy, high goodness of fit with the benchmark was observed for all four sub-models. Notably, RMSE values suggested marginal discrepancies < 0.05 m compared to benchmark results. This is because the optimised boundary conditions achieve more precise peak level predictions in downstream regions as opposed to the uniform closed-boundary conditions (maps showing the detailed benchmarking discrepancies for the four sub-model predictions are provided in Supplementary Document S5). For computing time comparisons, similar vector processing time was observed for the sub-impact zones screening procedure when targeting the different number of buildings. Compared to the benchmark, significant time reduction factors of 45-553 were yielded for the four sub-models. Yet, due to the difference in the generation of reduced domains (e.g. modelling grid extent and total No. of computational cells), time-savings for each sub-model differ from one case to another, demonstrating the case dependency (targets-specified) of this approach. In general, the sub-model approach provides robust performance when processing onto different terrain morphologies as well as different rainfall return periods. Thus, it is a feasible approach to reducing the computing time for 2D models.

https://doi.org/10.5194/hess-2020-243
Preprint. Discussion started: 30 July 2020


Hydrology and Earth System Sciences
Discussions
Open Access
EGU

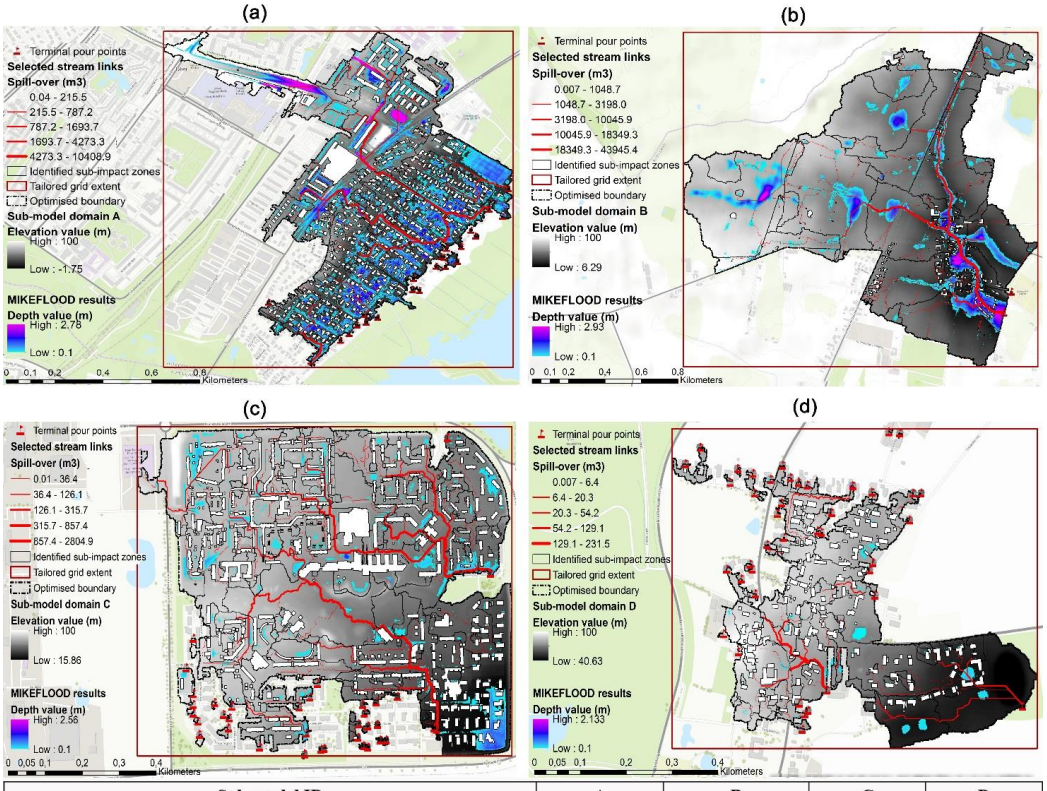


| Sub-model ID | | | A | B | C | D |
|---|---|---|---|---|---|---|
| Focus areas | Total No. of targeting buildings | | 784 | 254 | 757 | 382 |
| | Terrain morphologies | Avg. slope ± St. Dev. slope | 2.52 ± 3.76 | 1.40 ± 1.32 | 3.14 ± 4.71 | 3.30 ± 4.78 |
| | | Avg. El. ± St. Dev. El. (m) | 2.19 ± 1.02 | 14.73 ± 2.75 | 24.92 ± 2.75 | 50.23 ± 4.63 |
| Precipitations | Rain gauges and total rainfall amounts | | I5804(85.8mm):34% V5805(98.6mm):66 % | V5805(98.6mm):1% M5810(52.8mm):86% H5815(25.4mm):13% | H5815(25.4mm) | V5859(11.7mm) |
| | Return periods | | 100-yr | 50-yr | 10-yr | 1-yr |
| | Data volumes (MB) | | 579 | 909 | 210 | 130 |
| 1D flow conditions | Longest 1D flow length (m) (Tracing distance) | | 1,641 | 2,535 | 1,324 | 405 |
| | Max. spill-over volumes ($m^3$) | | 10,408.9 | 43,945.4 | 2,804.9 | 231.5 |
| | Total No. of identified sub-impact zones | | 188 | 154 | 273 | 121 |
| | Total areas of identified sub-impact zones ($m^2$) | | 677,781 | 1,676,207 | 485,508 | 151,893 |
| Sub-model domains | Tailored grid extent (Columns × Rows) | | 906 × 969 | 1217 × 1129 | 632 × 505 | 499 × 403 |
| | Total No. of computational cells (wet) | | 271,280 | 661,834 | 194,906 | 64,064 |
| MIKEFLOOD's 2D prediction discrepancies | Max. depth flood extent (Depth threshold of 0.01m) | $F^2$ | 0.980 | 0.990 | 0.966 | 0.880 |
| | Max. flood depth (m) | Max. | 0.433 | 0.098 | 0.106 | 0.094 |
| | | Mini. | -0.292 | -0.420 | -0.190 | -0.360 |
| | | Mean | -0.0002 | 0.0005 | -0.001 | -0.002 |
| | | RMSE | 0.015 | 0.003 | 0.008 | 0.015 |
| Computational time | Phase I (s) | Raster processing | 2,321 | | | |
| | | Vector processing | 111 | 146 | 181 | 144 |
| | Phase II (s) | Elapsed time | 6,196 | 10,654 | 2,413 | 873 |
| | | Time reduction factor | 78 | 45 | 200 | 553 |
| | | Time step | 0.2 | | | |

Basemap source: Esri, DigitalGlobe, GeoEye, Earthstar Geographics, CNES/Airbus DS, USDA, USGS, AEX, 724 Getmapping, Aerogrid, IGN, IGP, swisstopo, and the GIS User Community

Fig. 14. Four sub-models' 1D flow conditions, identified computational domains and their correspondent MIKE FLOOD predictions based on various types of terrain morphologies and rainfall return periods in 1-100 years: (a) Sub-model A, (b) Sub-model B, (c) Sub-model C and (d) Sub-model D. The optimised boundary conditions suggested by the sub-model approach are used for four sub-model simulations, where 2D outlets are established at the terminal pour points position that allows for water spilling at the pour point level. The detailed inputs, outputs, prediction validation and computational time information for each sub-model are provided in the table.

https://doi.org/10.5194/hess-2020-243
Preprint. Discussion started: 30 July 2020


Hydrology and Earth System Sciences
Discussions

## 5 Discussion

The presented method can tailor 2D grids based on various specified targets, which results in cost-efficient tailor-made sub-models. The strengths, weaknesses and associated potentials are discussed as follows:

Firstly, as suggested by the domain reduction tests, the criteria determining critical cells may affect 2D flow patterns substantially. Here, the sub-model approach identifies critical cells that indicate main flow paths (channel-flows) and corresponding catchment areas (sheet-flows) explicitly, whilst multiple terminal pour points are sufficiently detected and accommodated with suitable hydraulic alternatives (i.e. 2D weirs). At this point, the domains ensure accurate 2D replications of actual flow patterns. Yet, when using the criteria based on municipality borders, this domain - due to the exclusion of the critical inflow path cell (upstream) and the inclusion of irrelevant catchment cells (downstream) – may result in flood underestimations, as well as shifted positions for the terminal pour points. In this sense, the inundation simulation has failed to reproduce the actual flow pattern in the first place, such that the subsequent 2D predictions are questionable. For the same reason, the reduced domains based on other criteria, i.e. cutting off elevation cells greater than a certain threshold or making a buffer at a certain spatial distance, may be problematic. Thus, we conclude that, without perceiving the surface runoff network from a broad basin perspective, the determined domains most likely alter the actual flow pattern to various extents. As opposed to other criteria exclusively based on flow directions (i.e. ArcGIS' Basin/Watershed tool or Arc-Malstrøm's tracing functions), the sub-model approach further includes new criteria of the mass balance by enabling the 1D static flow routing, thus facilitating more valid domain reductions for the large-scale case area. However, these two approaches may result in identical domains in case that catastrophic events pose basin-wise spilling configurations. Here, a GIS-based automated tool that determines an optimal 1D/2D hybrid surface modelling strategy by replacing secondary important 2D surface components (grids) with 1D surface hydraulic alternatives is considered as a future solution to reduce the computational time even further (Allitt et al., 2009).

Secondly, the sub-model approach yields substantial time-savings by eliminating the domain irrelevant to specific targets. To pursue the desired computational efficiency, modellers may sharpen their focus by

https://doi.org/10.5194/hess-2020-243
Preprint. Discussion started: 30 July 2020


Hydrology and Earth System Sciences
Discussions

prioritising a few critical ones, as a limited number of target objects may result in more valid domain reductions, i.e. more time-savings. In contrast to the full-domain approach that implies general modelling targets, this targets-specified strategy may fail to provide the flood information outside the focus areas. Yet, based on distinct targets, the sub-model approach decomposes a large-scale model into many independent small sub-models (e.g. Sub-model A, B, C and D), and their computational independency would allow for parallel processing of multiple sub-models in a computer cluster environment without further accounting for flow interactions across their domain boundaries, thus reducing the computing time significantly. As another alternative solution, modellers may also adopt coarse-girds approach to fast complementing the predictions results other than the prioritised domains, and the final large-scale flood results fused from two parallel simulations (i.e. fine/coarse grids) should provide sufficient information whilst maintaining a marginal increase in overall computing time. Furthermore, due to the automation of the GIS-based procedure, the sub-model approach integrated with a real-time weather radar system may increase the possibility of applying 2D models into real-time forecasting applications in future. In this case, unlike a 'one for all' forecasting approach where predictive results of all possible future scenarios are provided based on one calibrated model, the sub-model approach would enable a more feasible forecasting solution in the adaption of real-world dynamics by reducing the scenario uncertainties through a real-time sub-model generation process.

Finally, the sub-model approach deploys a multiple-scale simulation strategy to obtain final predictions stepwise. From excluding different incidental representation processes according to the modelling purposes (i.e. aims i/ii, Section 1.3) specified for the two phases separately, sub-model approach uses different routings (i.e. 1D static/ 2D dynamic flows) with different complexities (i.e. hydrological/inundation process) at multiple scales (i.e. local catchment/ basin). Thus, the overall procedure achieves holistic computational efficiency compared to a single-time as-realistic-as-possible simulation for the large-scale inundation event. Further, without having additional efforts for code modifications in numeric engines, the implementation of the sub-model approach on other full 2D models should be straightforward. As most existing full 2D models perform similar peak water level predictions with marginal discrepancies in dense urban areas (Néelz and Pender, 2010), it is anticipated that the obtained validation results (Section 4.1.1, 4.1.2) proven based on MIKE

https://doi.org/10.5194/hess-2020-243
Preprint. Discussion started: 30 July 2020


Hydrology and Earth System Sciences
Discussions

FLOOD should fit for other full 2D engines – at least for the peak water levels. Yet, due to the various ways of coding velocity in full 2D models, the validation results for velocity hydrographs represent for MIKE FLOOD only. In addition, this approach is initially designed for dealing with flood inundation process dominated by overland flows. However, when rainfall amounts are low, the enhanced influence of the underground drainage system may affect the overland flow continuity, thus affecting domain reductions. For the sake of this limitation, adding a drainage component to represent the drainage system comprehensively could be an interesting future development, and further investigations on the significance of drainage systems regarding 1D flow continuity should be addressed. In addition, the sinks' spill-overs in the current sub-model approach are simplified as "static" and single direction spilling. Therefore, incorporating a dynamic 1D routing (dynamic wave/kinematic wave) and a multiple-direction-spilling component would add more accuracy to flow pattern representations, thus ensuring more precise domain reductions. However, the trade-off between the modelling complexity, the computing time and the enhanced accuracy should be addressed and ultimately balanced based on the specified modelling purpose.

## 6. **Conclusion**

This paper presents a targets-specified grids-tailored sub-model approach to reducing the computing time for large-scale high-resolution 2D urban flood modelling. By utilising the enabled 1D static flows to trace sub-impact zones relevant to specific target objects, critical computational cells, that configure reduced computation domains as well as optimised boundary conditions, are extracted from a full-basin DEM's high-resolution grids for MIKE FLOOD simulations. The outcome is tailor-made sub-models that require less computational efforts while avoiding significant losses in the prediction accuracy. The proposed method was tested for a basin area, the impacts of domain reductions and optimised boundary conditions on MIKE FLOOD were validated, and the general applicability and robustness of the suggested method were tested by targeting four focus areas accounting for different rainfalls as well as different terrain morphologies. The main findings are outlined as follow:

- The proposed sub-model approach performs 45-553 times faster processing in MIKE FLOOD by reducing 99% computational cells deemed to be irrelevant according to specified targets, i.e. specific

https://doi.org/10.5194/hess-2020-243
Preprint. Discussion started: 30 July 2020


Hydrology and Earth System Sciences
Discussions

685 buildings and specified precipitations; Domain reduction tests reveal minor discrepancies against the
686 benchmark (i.e. full-basin domain) concerning peak water levels when using the sub-model approach,
687 and the general error deviations are within marginal level of < 0.05 m. The internal point hydrographs
688 indicate general consistent spatial-temporal variations in water depths and flow velocities. Due to the
689 violation of the actual flow pattern, differences were found in u- and v-velocities. However, the
690 boundary condition comparison test reveals that the optimised boundary conditions resolve these
691 potential errors properly. As suggested by the general applicability test, the performance of the sub-
692 model approach is robust when dealing with different terrain morphologies as well as different rainfall
693 return periods, whilst their RMSE are maintained at the marginal level of < 1.5 cm.

694 • Domains configured by critical cells impact the final 2D predictions substantially. The sub-model
695 approach incorporates relevant flow patterns explicitly by tracing 1D static routing and accommodates
696 commensurate hydraulic alternatives (i.e. 2D weirs) at terminal pour point positions, thus ensuring
697 precise representations of actual flow patterns in configured 2D domain compared to other approaches.
698 As opposed to the full-domain approach that implies general modelling targets, the sub-model
699 approach provides no flood information outside the focus areas. However, the independency in-
700 between various sub-models is a substantial advantage to parallel process many small sub-models in
701 computer cluster environments without further considering information interactions across domain
702 boundaries. Alternatively, modellers are recommended to use coarse grids to complement flood
703 predictions beyond the prioritised domains. We see the two options as feasible solutions to improve
704 computing time even further.

705 • With a multiple-scale simulation strategy, the sub-model approach decomposes a computationally
706 expensive large-scale simulation process into two phases by emphasizing appropriate modelling
707 complexities at multiple scales, which results in a holistic modelling efficiency. Besides, without
708 reprogramming existing codes in numeric engines, the implementation of the sub-model approach on
709 other full 2D models is straightforward. Furthermore, with the automation of the GIS-based procedure,


710 the sub-model approach is considered as a promising solution to the realisation of the 2D real-time
711 forecasting system when integrated with a real-time weather radar system.

712 **Author contribution**

713 Guohan Zhao: Conceptualization, Methodology, Software, Validation, Formal analysis, Data Curation,
714 Visualization, Writing – Original Draft & Editing, Funding acquisition.

715 Thomas Balstrøm: Writing – Review & Editing, Resources, Supervision, Software.

716 Ole Mark: Writing – Review & Editing, Resources, Supervision, Validation.

717 Marina Bergen Jensen: Writing – Review & Editing, Resources, Supervision, Project administration, Funding
718 acquisition.

719 **Competing interests**

720 The authors declare that they have no conflict of interest.

721 **Acknowledgements**

722 Guohan Zhao is sponsored by the Chinese Scholar Council [CSC NO. 201507000058]. DHI is acknowledged
723 for granting access to the MIKE FLOOD license. The authors would like to thank the editors and anonymous
724 reviewers who provides valuable comments and constructive suggestions to this article.

725 **Reference:**

726 Allitt, R., Blanltsby, J., Djordjević, S., Maksimović, Č., Stewart, D., 2009. Investigations into 1D-1D and 1D-
727 2D urban flood modelling - UKWIR project. Presented at the WaPUG Autumn Conference 2009,
728 Blackpool, UK.

729 Arge, L., Revsbæk, M., Zeh, N., 2010. I/O-efficient computation of water flow across a terrain. Sym. Comput.
730 Geom. DOI:10.1145/1810959.1811026

731 Baker, W.L., Cai, Y., 1992. The r. le programs for multiscale analysis of landscape structure using the GRASS
732 geographical information system. Landesc. Ecol., 7(4): 291-302. https://doi.org/10.1007/BF00131258

733 Balstrøm, T., Crawford, D., 2018. Arc-Malstrøm: A 1D hydrologic screening method for stormwater
734 assessments based on a geometric network. Comput. Geosci., 116: 64–73.
735 https://doi.org/10.1016/j.cageo.2018.04.010

https://doi.org/10.5194/hess-2020-243
Preprint. Discussion started: 30 July 2020




736 Barnea, S., Filin, S., 2008. Keypoint based autonomous registration of terrestrial laser point-clouds. ISPRS J.
737 Photogramm. Remote Sens., 63(1): 19-35. https://doi.org/10.1016/j.isprsjprs.2007.05.005
738 Bates, P.D., Horritt, M.S., Smith, C., Mason, D.C., 1997. Integrating remote sensing observations of flood
739 hydrology and hydraulic modelling. Hydrol. Process., 11(14): 1777-1795.
740 https://doi.org/10.1002/(SICI)1099-1085(199711)11:14<1777::AID-HYP543>3.0.CO;2-E
741 Bates, P.D., Horritt, M.S., Fewtrell, T.J., 2010. A simple inertial formulation of the shallow water equations
742 for efficient two-dimensional flood inundation modelling. J. Hydrol., 387(1): 33-45.
743 https://doi.org/10.1016/j.jhydrol.2010.03.027
744 Bernini, A., Franchini, M., 2013. A rapid model for delimiting flooded areas. Water Resour. Manage., 27(10):
745 3825-3846. https://doi.org/10.1007/s11269-013-0383-3
746 Bernstein, L., Bosch P., Canziani O., Chen Z., Christ R., Riahi K., 2008. IPCC, 2007: climate change 2007:
747 synthesis report. IPCC.
748 Bruwier, M., Archambeau, P., Erpicum, S., Pirotton, M., Dewals, B., 2017. Shallow-water models with
749 anisotropic porosity and merging for flood modelling on Cartesian grids. J. Hydrol., 554: 693-709.
750 https://doi.org/10.1016/j.jhydrol.2017.09.051
751 Chen, A.S., Evans, B., Djordjević, S., Savić, D.A., 2012a. A coarse-grid approach to representing building
752 blockage effects in 2D urban flood modelling. J. Hydrol., 426: 1-16.
753 https://doi:10.1016/j.jhydrol.2012.01.007
754 Chen, A.S., Evans, B., Djordjević, S., Savić, D.A., 2012b. Multi-layered coarse grid modelling in 2D urban
755 flood simulations. J. Hydrol., 470: 1-11. https://doi.org/10.1016/j.jhydrol.2012.06.022
756 Chen, J., Hill, A.A., Urbano, L.D., 2009. A GIS-based model for urban flood inundation. J. Hydrol., 373(1):
757 184-192. https://doi.org/10.1016/j.jhydrol.2009.04.021
758 Cobby, D.M., Mason, D.C., Horritt, M.S., Bates, P.D., 2003. Two-dimensional hydraulic flood modelling
759 using a finite-element mesh decomposed according to vegetation and topographic features derived
760 from airborne scanning laser altimetry. Hydrol. Process., 17(10): 1979-2000.
761 https://doi.org/10.1002/hyp.1201

https://doi.org/10.5194/hess-2020-243
Preprint. Discussion started: 30 July 2020




[dataset] Danish Geodata Agency, 2015. Product specification. Denmark's elevation model, DHM/Terrain (in Danish), Copenhagen.

[dataset] Data Supply and Efficiency Board, 2013. DHM/Nedbør, Copenhagen.

DHI Water & Environment, 2017. MIKE FLOOD User Manual. DHI Software, Hørsholm, Denmark.

Dottori, F., Todini, E., 2010. A 2D flood inundation model based on cellular automata approach. Presented at XVIII International Conference on Water Resources CMWR. Barcelona.

Dottori, F., Todini, E., 2011. Developments of a flood inundation model based on the cellular automata approach: testing different methods to improve model performance. Phys. Chem. Earth, Parts A/B/C, 36(7): 266-280. https://doi.org/10.1016/j.pce.2011.02.004

Esri, 2019. http://desktop.arcgis.com/en/arcmap/latest/manage-data/geometric-networks/what-are-geometric-networks-.htm.

Fewtrell, T.J., Bates, P.D., Horritt, M.S., Hunter, N.M., 2008. Evaluating the effect of scale in flood inundation modelling in urban environments. Hydrol. Process., 22(26): 5107-5118. https://doi.org/10.1002/hyp.7148

Fewtrell, T.J., Duncan, A., Sampson, C.C., Neal, J.C., Bates, P.D., 2011. Benchmarking urban flood models of varying complexity and scale using high resolution terrestrial LiDAR data. Phys. Chem. Earth, Parts A/B/C, 36(7): 281-291. https://doi.org/10.1016/j.pce.2010.12.011

Ghimire, B., Chen, A.S., Guidolin, M., Keedwell, E.C., Djordjević, S., Savić, D.A., 2013. Formulation of a fast 2D urban pluvial flood model using a cellular automata approach. J. Hydroinform., 15(3): 676-686. https://doi.org/10.2166/hydro.2012.245

Glenis, V., McGough, A.S., Kutija, V., Kilsby, C., Woodman, S., 2013. Flood modelling for cities using Cloud computing. J. Cloud Comput.: Adv., Syst. Appl., 2(1): 7. https://doi.org/10.1186/2192-113X-2-7

Gouldby, B., Sayers, P., Mulet-Marti, J., Hassan, M., Benwell, D., 2008. A methodology for regional-scale flood risk assessment, Proc. ICE - Water Manage. 161(3): 169-182. https://doi.org/10.1680/wama.2008.161.3.169

Greenlee, D.D., 1987. Raster and vector processing for scanned linework. Photogramm. Eng. Remote Sens., 53: 1383-1387.



789 Guidolin, M., Chen, A.S., Ghimire, B., Keedwell, E.C., Djordjević, S., Savić, D.A., 2016. A weighted cellular
790 automata 2D inundation model for rapid flood analysis. Environ. Modell. Softw., 84: 378-394.
791 https://doi.org/10.1016/j.envsoft.2016.07.008
792 Guinot, V., Soares-Frazão, S., 2006. Flux and source term discretization in two-dimensional shallow water
793 models with porosity on unstructured grids. Internation. J. Numeri. Methods Fluids, 50(3): 309-345.
794 https://doi.org/10.1002/fld.1059
795 Hansson K., H.F., Grauert M., Larsen M., 2010. THE BLUE SPOT CONCERT: Methods to predict and
796 handle flooding on highway systems in lowland areas. Report 181-2010, Danish Road Institute,
797 Hedehusene, Demark.
798 Hénonin, J., Hongtao, M., Zheng-Yu, Y., Hartnack, J., Havnø, K., Gourbesville, P., Mark, O., 2015. Citywide
799 multi-grid urban flood modelling: the July 2012 flood in Beijing. Urban Water J., 12(1): 52-
800 66. https://doi.org/10.1080/1573062X.2013.851710
801 Hunter, N.M., Bates, P.D., Neelz, S., Pender, G., Villanueva, I., Wright, N.G., Liang, D., Falconer, R.A., Lin,
802 B., Waller, S., Crossley, A.J., Mason, D.C., 2008. Benchmarking 2D hydraulic models for urban flood
803 simulations, Proc. ICE - Water Manage. 161(1):13-30. https://doi.org/10.1680/wama.2008.161.1.13
804 Hunter, N.M., Bates, P.D., Horritt, M.S., Wilson, M.D., Simple spatially-distributed models for predicting
805 flood inundation: a review, Geomorphology, 90 (2007), pp. 208-225.
806 https://doi.org/10.1016/j.jhydrol.2010.03.027
807 Jahanbazi, M., Egger, U., 2014. Application and comparison of two different dual drainage models to assess
808 urban flooding. Urban Water J., 11(7). https://doi.org/10.1080/1573062X.2013.871041
809 Jamali, B., Löwe, R., Bach, P. M., Urich, C., Arnbjerg-Nielsen, K., Deletic, A., 2018. A rapid urban flood
810 inundation and damage assessment model. J. Hydrol., 564: 1085-1098.
811 https://doi.org/10.1016/j.jhydrol.2018.07.064.
812 Jensen, L.N., Paludan, B., Nielsen, N.H., Edinger, K., 2010. Large scale 1D-1D surface modelling tool for
813 urban water planning. Presented at the Novatech International Conference on Sustainable
814 Technologies and Strategies in Urban Water Management, Lyon, France.

https://doi.org/10.5194/hess-2020-243
Preprint. Discussion started: 30 July 2020




815 Jenson, S.K., Domingue, J.O., 1988. Extracting topographic structure from digital elevation data for
816 geographic information system analysis. Photogramm. Eng. Remote Sens., 54(11): 1593-1600.
817 Krupka, M., Pender, G., Wallis, S., Sayers, P.B., Marti, J.M., 2007. A rapid flood inundation model. Presented
818 at International Association for Hydro-Environment Engineering and Research. Venice, Italy.
819 Kuiry, S.N., Sen, D., Bates, P.D., 2010. Coupled 1D–quasi-2D flood inundation model with unstructured grids.
820 J. Hydrol. Eng., 136(8): 493-506. https://doi.org/10.1061/(ASCE)HY.1943-7900.0000211
821 Lamb, R., Crossley, M., Waller, S., 2009. A fast two-dimensional floodplain inundation model, Proc. ICE -
822 Water Manage., 162(1): 1-9. https://doi.org/10.1680/wama.2009.162.6.363
823 Leandro, J., Chen, A.S., Djordjević, S., Savić, D.A., 2009. Comparison of 1D/1D and 1D/2D coupled
824 (sewer/surface) hydraulic models for urban flood simulation. J. Hydraul. Eng., 135(6): 495-504.
825 https://doi.org/10.1061/(ASCE)HY.1943-7900.0000037
826 Leitão, J.P., Boonya-aroonnet, S., Prodanović, D., Maksimović, Č., 2009. The influence of digital elevation
827 model resolution on overland flow networks for modelling urban pluvial flooding. Water Sci.
828 Technol., 60(12): 3137-3149. https://doi.org/10.2166/wst.2009.754
829 Leitão, J.P., Moy de Vitry, M., Scheidegger, A., Rieckermann, J. 2016. Assessing the quality of digital
830 elevation models obtained from mini unmanned aerial vehicles for overland flow modelling in urban
831 areas. Hydrol. Earth Syst. Sci. Discuss., 12(6): 5629-5670. https://doi.org/10.5194/hess-20-1637-2016
832 Lhomme, J., Sayers, P.B., Gouldby, B.P., Samuels, P.G., Wills, M., Mulet-Marti, J., 2008. Recent development
833 and application of a rapid flood spreading method. FLOODrisk2008 Flood Risk Management:
834 Research and Practice, Taylor & Francis Group, Keble College, Oxford(2008), pp. 15-24.
835 Lichti, D.D., Pfeifer, N., Maas, H.-G., 2008. Editorial: ISPRS journal of photogrammetry and remote sensing
836 theme issue “Terrestrial Laser Scanning”, ISPRS J. Photogram. Remote. Sens. 63, 1-3.
837 Lindsay, J.B., Creed, I.F., 2006. Distinguishing actual and artefact depressions in digital elevation data.
838 Comput. Geosci., 32(8): 1192-1204. https://doi.org/10.1016/j.cageo.2005.11.002
839 Liu, Y., Pender, G., 2010. A new rapid flood inundation model, Presented at the International Association for
840 Hydro-Environment Engineering and Research European Congress, Edinburgh, UK.

https://doi.org/10.5194/hess-2020-243
Preprint. Discussion started: 30 July 2020




841 Maksimović, Č., Prodanović, D., Boonya-aroonnet, S., Leitão, J.P., Djordjević, S., Allitt, R., 2009. Overland
842 flow and pathway analysis for modelling of urban pluvial flooding. J. Hydraul. Res., 47(4): 512-523.
843 https://doi.org/10.1080/00221686.2009.9522027
844 Mark, O., Parkinson, J., 2005. The future of urban storm management: an integrated approach. Water, 21(8):
845 30–32.
846 Mark, O., Weesakul, S., Apirumanekul, C., Boonya-aroonnet, S., Djordjević, S., 2004. Potential and
847 limitations of 1D modelling of urban flooding. J. Hydrol., 299(3-4): 284-299.
848 https://doi.org/10.1016/j.jhydrol.2004.08.014
849 Marks, K., Bates, P.D., 2000. Integration of high-resolution topographic data with floodplain flow models.
850 Hydrol. Process., 14(11-12): 2109-2122.
851 Mason, D.C., Cobby, D.M., Horritt, M.S., Bates, P.D., 2003. Floodplain friction parameterization in two-
852 dimensional river flood models using vegetation heights derived from airborne scanning laser
853 altimetry. Hydrol. Process., 17(9): 1711-1732. https://doi.org/10.1002/hyp.1270
854 Mason, D.C., Horritt, M.S., Hunter, N.M., Bates, P.D., 2007. Use of fused airborne scanning laser altimetry
855 and digital map data for urban flood modelling. Hydrol. Process., 21(11): 1436-1447. https://doi.org/
856 10.1002/hyp.6343
857 McMillan, H.K., Brasington, J., 2007. Reduced complexity strategies for modelling urban floodplain
858 inundation. Geomorphol., 90(3): 226-243. https://doi.org/10.1016/j.geomorph.2006.10.031
859 Meesuk, V., Vojinovic, Z., Mynett, A.E., Abdullah, A.F., 2015. Urban flood modelling combining top-view
860 LiDAR data with ground-view SfM observations. Adv. Water Resour., 75: 105-117.
861 https://doi.org/10.1016/j.advwatres.2014.11.008
862 Neal, J.C., Fewtrell, T.J., Trigg, M., 2009. Parallelisation of storage cell flood models using OpenMP. Environ.
863 Modell. Softw., 24(7): 872-877. https://doi.org/10.1016/j.envsoft.2008.12.004
864 Neal, J.C., Fewtrell, T.J., Bates, P.D., Wright, N.G., 2010. A comparison of three parallelisation methods for
865 2D flood inundation models. Environ. Modell. Softw., 25(4): 398-411.
866 https://doi.org/10.1016/j.envsoft.2009.11.007

https://doi.org/10.5194/hess-2020-243
Preprint. Discussion started: 30 July 2020


Hydrology and Earth System Sciences
Discussions

867 Néelz, S., Pender, G., 2010. Benchmarking of 2D hydraulic modelling packages. Heriot-Watt University,
868 Edinburgh.
869 Sampson, C.C., Fewtrell, T.J., Duncan, A., Shaad, K., Horritt, M.S., Bates, P.D., 2012. Use of terrestrial laser
870 scanning data to drive decimetric resolution urban inundation models. Adv. Water Resour., 41: 1-17.
871 https://doi.org/10.1016/j.advwatres.2012.02.010
872 Sanders, B.F., Schubert, J.E., Gallegos, H.A., 2008. Integral formulation of shallow-water equations with
873 anisotropic porosity for urban flood modeling. J. Hydrol., 362(1-2): 19-38.
874 https://doi.org/10.1016/j.jhydrol.2008.08.009
875 Schmitt, T.G., Thomas, M., Ettrich, N., 2004. Analysis and modeling of flooding in urban drainage systems.
876 J. Hydrol., 299(3-4): 300-311. Https://doi.org/10.1016/j.jhydrol.2004.08.012
877 Schubert, J.E., Sanders, B.F., Smith, M.J., Wright, N.G., 2008. Unstructured mesh generation and landcover-
878 based resistance for hydrodynamic modeling of urban flooding. Adv. Water Resour., 31(12): 1603-
879 1621. https://doi.org/10.1016/j.advwatres.2008.07.012
880 Shaad, K., 2009. Surface water flooding: analysis and model development. MS thesis. Brandenburg University
881 of Technology, Cottbus, Germany.
882 Shreve, R. L., 1966. Statistical law of stream numbers, J. Geol. 74. 17-37.
883 Tokarczyk, P., Leitão, J.P., Rieckermann, J., Schindler, K., Blumensaat, F., 2015. High-quality observation of
884 surface imperviousness for urban runoff modelling using UAV imagery. Hydrol. Earth Syst. Sci.,
885 19(10): 4215-4228. https://doi.org/10.5194/hess-19-4215-2015
886 Werner, M., Hunter, N.M., Bates, P.D, 2005. Identifiability of distributed floodplain roughness values in flood
887 extent estimation. J. Hydrol., 314(1): 139-157. https://doi.org/10.1016/j.jhydrol.2005.03.012
888 Yu, D., 2010. Parallelization of a two-dimensional flood inundation model based on domain decomposition.
889 Environ. Modell. Softw., 25(8): 935-945. https://doi.org/10.1016/j.envsoft.2010.03.003
890 Yu, D., Coulthard, T.J., 2015. Evaluating the importance of catchment hydrological parameters for urban
891 surface water flood modelling using a simple hydro-inundation model. J. Hydrol., 524: 385-400.
892 https://doi.org/10.1016/j.jhydrol.2015.02.040

https://doi.org/10.5194/hess-2020-243
Preprint. Discussion started: 30 July 2020


Hydrology and Earth System Sciences
Discussions

893 Yu, D., Lane, S.N., 2006a. Urban fluvial flood modelling using a two-dimensional diffusion-wave treatment,
894 part 1: mesh resolution effects. Hydrol. Process., 20(7): 1541-1565. https://doi.org/10.1002/hyp.5935.
895 Yu, D., Lane, S.N., 2006b. Urban fluvial flood modelling using a two-dimensional diffusion-wave treatment,
896 part 2: development of a sub-grid-scale treatment. Hydrol. Process., 20(7): 1567-1583.
897 https://doi.org/10.1002/hyp.5936
898 Yu, D., Lane, S.N., 2011. Interactions between subgrid-scale resolution, feature representation and grid-scale
899 resolution in flood inundation modelling. Hydrol. Process., 25(1): 36-53.
900 https://doi.org/10.1002/hyp.7813
901 Zerger, A., Smith, D., Hunter, G., Jones, S., 2002. Riding the storm: a comparison of uncertainty modelling
902 techniques for storm surge risk management. Appl. Geogr., 22(3): 307-330.
903 https://doi.org/10.1016/S0143-6228(02)00010-3
904 Zhang, S., Pan, B., 2014. An urban storm-inundation simulation method based on GIS. J. Hydrol., 517: 260-
905 268. https://doi.org/10.1016/j.jhydrol.2014.05.044
906 Zhang, S., Wang, T., Zhao, B., 2014. Calculation and visualization of flood inundation based on a topographic
907 triangle network. J. Hydrol., 509: 406-415. https://doi.org/10.1016/j.jhydrol.2013.11.060